https://doi.org/10.5194/essd-2025-440
Preprint. Discussion started: 28 August 2025

Open Access Earth System Science Data Discussions

A multiyear eddy covariance and meteorological dataset from five pairs of agroforestry systems with open cropland or grassland in Northern Germany

José Ángel Callejas-Rodelas[1], Justus van Ramshorst[1,2], Alexander Knohl[1,3], Lukas Siebicke[1], Dietmar Fellert[1], Marek Peksa[1], Dirk Böttger[4], and Christian Markwitz[1]

[1]Bioclimatology, University of Göttingen, Göttingen, Germany
[2]Quanterra Systems Ltd., Centenary House, Peninsula Park, Exeter EX2 7XE, UK
[3]Centre for Biodiversity and Land Use, University of Göttingen, Göttingen, Germany
[4]Soil Science of Tropical and Subtropical Ecosystems, University of Göttingen, Göttingen, Germany

Correspondence: José Ángel Callejas-Rodelas (joseangel.callejasrodelas@uni-goettingen.de)

Abstract. Agroforestry systems are considered suitable nature-based solutions to mitigate climate change. Long-term measurements of CO_2 fluxes, evapotranspiration and sensible heat fluxes are, however, largely still missing. Here we present a unique eddy covariance and meteorological dataset from a total of ten stations paired over agroforestry and open cropland or grassland agricultural sites located in Northern Germany. The data were harmonized to create a consistent dataset which includes gap-filled time series of meteorological and lower-cost eddy covariance measurements with identical instrumentation, accounting for a total of seventy eight site-years of data. The objective of this dataset is to provide observational data on the differences of meteorological conditions, carbon, water and energy balances of adjacent agroforestry and open cropland or grassland sites in five distinct climatic regions of Germany. This extensive, continuous dataset can be used to study ecosystem properties and the potential benefits of agroforestry. It can also be used to parametrize models on crop and biomass productivity, or to evaluate the response of such agroecosystems to climate change scenarios, among other applications. Anticipated key users of this dataset are researchers in the fields of micrometeorology, eddy covariance, agronomy, and ecosystem modeling. This dataset can be accessed through https://doi.org/10.25625/A2Z8T8 (Callejas Rodelas et al., 2025b).

1 Introduction

The conversion of conventional agriculture, represented by open cropland (OC) or open grassland (OG) systems, to agroforestry (AF) systems, is an example of a nature-based solution with the potential to positively impact towards climate change mitigation (Cardinael et al., 2021; Chapman et al., 2020; Kay et al., 2019). AF encompasses any type of agricultural system in which trees and crops are cultivated concurrently, with the objective of benefiting from the presence of the trees in the agricultural land while keeping an agricultural production of food, timber or other products (Nair, 1985). AF systems traditionally have been

https://doi.org/10.5194/essd-2025-440
Preprint. Discussion started: 28 August 2025

an important component in many agricultural landscapes across the globe. These systems encompass a wide array of practices adapted to the requirements of the territories, climate, culture, society or economy (Pancholi et al., 2023). Intensive research has been conducted on AF systems to study their environmental benefits (for reviews on this topic, see Satish et al., 2024, Pancholi et al., 2023, Singh et al., 2021). Due to the demonstrated superior performance in ecosystem functions and services (Kay et al., 2019), there is an increasing interest in recent years to stimulate the transition of conventional agriculture to AF in numerous regions globally (Gupta et al., 2020).

AF systems have the potential to increase carbon sequestration, in comparison to conventional agriculture, in both within the soil (Cardinael et al., 2015, 2017) and via biomass growth (Peichl et al., 2006). According to De Stefano and Jacobson (2017), soil organic carbon (SOC) stocks exhibited an increase at several sites that had transitioned from agricultural to agroforestry land use. Moreover, AF systems can also increase water use efficiency (*WUE*) (Ong et al., 2002), as ecosystem-scale evapotranspiration (ET) is expected to stay equal (Markwitz et al. (2020a), even under increased CO_2 uptake. *WUE* is defined as the amount of carbon assimilated as biomass or grain produced per unit of water used by the crop (Hatfield and Dold, 2019), which is equivalent to Gross Primary Production (*GPP*) divided by evapotranspiration ($WUE = GPP\ /\ ET$).

Short Rotation Alley Cropping (SRAC) is a type of AF in which trees and crops are cultivated in parallel (Markwitz and Siebicke, 2019). There is an increasing interest in such agricultural systems in regions like central Europe (Quinkenstein et al., 2009). Crops rotate in seasonal cycles, while trees rotate in periods of typically 3 to 6 years and are used for biomass production, e.g. for bioenergy (Böhm et al., 2014). Therefore, these systems can provide a renewable source of energy, while still keeping a relatively large yield production from the crops (Veldkamp et al., 2023). In order to thoroughly address the impact of such land use conversion, further data are required, that quantify ecosystem-atmosphere interactions at the system in order to understand how AF impacts the surface energy balance, carbon sequestration, evapotranspiration, and *WUE*.

The eddy covariance (EC) technique has become the main tool for the study of land-atmosphere interactions at the ecosystem scale (Baldocchi, 2014). EC allows to quantify ecosystem-scale exchanges of energy, trace gases and momentum between ecosystems and the atmosphere. However, there are inherent challenges in its application, including the costs of installation and maintenance (Hill et al., 2017), data storage and management (Aubinet et al., 2012), and data processing with complex data pipelines (Sabbatini et al., 2018; Pastorello et al., 2020). This has led to a lack of direct measurements with the EC technique over certain types of ecosystems in recent decades (Schimel et al., 2015), including AF systems and, specifically, SRAC systems (Markwitz and Siebicke, 2019).

Most of the research on carbon, water and energy balances of AF systems has been performed in tropical areas (Cardinael et al., 2015), where AF systems have a higher socio-economic and environmental significance (Chapman et al., 2020), and not in temperate regions. For illustrative purposes, the reader is referred to e.g. Chinchilla-Soto et al. (2021) or Gomez-Delgado et al. (2011). Furthermore, the studies conducted in the temperate zone have mainly focused on evaluating the potential carbon sequestration of an AF system by studying soil composition and SOC (e.g. Kanzler et al., 2021; Cardinael et al., 2015; Howlett et al., 2011); by combining *in situ* measurements of SOC, C leaching and respiration with models to assess ecosystem-level C pools (e.g. Peichl et al., 2006) or by assessing aboveground biomass in AF systems using remote sensing (Sprenkle-Hyppolite et al., 2024; Zomer et al., 2016). However, none of these studies directly measured ecosystem-scale CO_2 or H_2O exchanges

https://doi.org/10.5194/essd-2025-440
Preprint. Discussion started: 28 August 2025

via the EC technique. To the best of our knowledge, the study of Ward et al. (2012) was the only one that quantified carbon and water balances of an alley cropping AF using EC, in a Mediterranean climate in Australia.

As part of the SIGNAL project (http://www.signal.uni-goettingen.de/subprojects/tp1-2-evapotranspiration/, last accessed 29 October 2024), the study by Markwitz et al. (2020a) quantified ecosystem-scale energy and water flux densities and the influence of SRAC on evapotranspiration using the EC technique. Two studies have evaluated the lower-cost EC setups used for this dataset (Callejas-Rodelas et al., 2024; van Ramshorst et al., 2024). Another study was published, focusing on carbon exchanges over some of the studied sites for the period 2019-2021 (van Ramshorst et al., 2025). Furthermore, a recent study investigated the spatial variability of carbon and water flux densities across one of the SRAC systems involved in the project (Callejas-Rodelas et al., 2025a).

This study presents multiple years of data concerning land-atmosphere exchange processes, as measured during the SIGNAL project. The dataset covers meteorological data, EC flux density time series of CO_2, H_2O, sensible heat (H), latent heat (LE) and momentum, some of the main measured turbulent flow variables (standard deviation of vertical wind velocity, *SIGMA_W*, friction velocity, *USTAR*, Obukhov length, *MO_LENGTH*), and footprint climatology. We provide a unique, harmonized dataset, incorporating the most significant variables recorded at the paired OC or OG and SRAC sites. The datasets can be used for different purposes, with the main targets being the micrometeorological and the modeling scientific communities. Good quality-controlled long-term data above SRAC and OC/OG sites can be a highly valuable input for models aiming to predict crop and land-use change responses under different climate change scenarios. Furthermore, these data, in conjunction with other datasets that compare the ecosystem functioning between AF and OC/OG, can be used by stakeholders and decision-makers in the development of agricultural policy.

2 Methods and datasets description

2.1 Site description

The study sites were located in Northern Germany in five different regions (Fig. 1): Dornburg (51.015 °N, 11.64 °E, Thuringia), Forst (51.79 °N, 14.63 °E, Brandenburg), Mariensee (52.565 °N, 9.464 °E, Lower Saxony), Vechta (52.759 °N, 8.549 °E, Lower Saxony) and Wendhausen (52.33 °N, 10.632 °E, Lower Saxony). The mean annual temperature and precipitation for the reference period (1981-2010) for all regions is shown in Table 1, with values extracted from the German Weather Service data portal (DWD, 2024). The IDs of the DWD stations closest to the sites are Jena (2444), Cottbus (880), Hanover (2014), Grossenkneten (44) and Brunswick Airport (662), respectively. For simplicity, the SRAC systems will henceforth be referred to as AF.

Each study region was divided into an AF and a OC or OG site. AF consisted of tree strips of fast-growing species, which were intercalated by crops, for Dornburg, Forst, Vechta and Wendhausen; or by perennial grassland, for Mariensee. Trees were poplar (*Populus Nigra x Populus Maximowiczii*) in Dornburg, Vechta and Wendhausen, while they were willow (*Salix schwerinii x S. viminalis*) in Mariensee, and both poplar and black locust (*Robinia pseudoacacia*) in Forst. The management of crops or grass at both OC or OG and AF was similar. Crops were subject to a yearly rotation scheme, while trees were typically

https://doi.org/10.5194/essd-2025-440
Preprint. Discussion started: 28 August 2025

Open Access Earth System Science Data Discussions

Table 1. Site location, climatological averages and standard deviations of annual air temperature (*TA*) and annual sum of precipitation (*P*) for the reference period 1981-2010 (DWD, 2024), elevation above sea level and soil characteristics, for all the project sites. Soil type and organic carbon content are based on Shao et al. (2025), Veldkamp et al. (2023) and Schmidt et al. (2021), while soil bulk density is based on Shao et al. (2025) and Markwitz et al. (2020a).

	Dornburg	Forst	Mariensee	Vechta	Wendhausen
Location	51°00’50" N 11°38’38" E	51°47’20" N 14°37’57" E	52°33’51" N 09°27’51" E	52°45’33" N 08°32’59" E	52°19’59" N 10°37’53" E”
Mean *TA* (°C)	9.9 ± 0.8	9.6 ± 0.8	9.6 ± 0.8	9.3 ± 0.8	9.6 ± 0.9
Mean *P* (mm)	608 ± 117	568 ± 117	661 ± 109	806 ± 139	637 ± 125
Elevation a.s.l (m)	289	66	42	43	82
Soil type	Calcaric Phaeozem	Gleyc Cambisol	Anthrosol	Sandy Aeronosol	Vertic Cambisol
Soil organic carbon (kg C m^{-2})	4.64	3.48	22.5	6.9	6.16
Soil bulk density (Mg m^{-3})	1.19	1.28	1.28	1.3	0.89

harvested in cycles of three to four years. Grass was cut twice per year in Mariensee. During the project, tree harvest took place in February of 2021 for Forst, Mariensee and Wendhausen. No tree cut happened in Vechta and in Dornburg. However, in Dornburg a partial cut of 15 m on each side of the EC station took place in winter 2018/19 to mitigate the potential impact of tall trees on the EC measurements. Table A1 shows the crops, sowing and harvest dates, and the harvest dates of trees, for all the sites from 2016 to 2024. Further information on the management can be found in the supplementary material of Veldkamp et al. (2023).

https://doi.org/10.5194/essd-2025-440
Preprint. Discussion started: 28 August 2025

Figure 1. Map of site location within Germany. The blue dot represents the grassland agroforestry site (Mariensee), while the red dots represent the cropland agroforestry sites (Dornburg, Forst, Vechta and Wendhausen).

Two EC stations were installed at each region, one at the AF site and one at the OC/OG site. At Wendhausen, two additional stations were installed at the AF from August of 2022 to September 2024. A detailed analysis of the distributed network of three stations above the AF is presented in (Callejas-Rodelas et al., 2025a). The present article focuses exclusively on the long-term dataset corresponding to the original paired AF and OC stations in Wendhausen, maintaining a similar structure to the other sites. The AF sites in Dornburg, Forst and Wendhausen, as well as the OC sites, were large in comparison to the stations' footprint area (Fig. 2a, b and c). In Mariensee, the AF site was small in comparison to the footprint area (Fig. 2c). In Vechta, the footprint area covered by the AF station was small because of the tall surrounding trees located in the western and southern sectors (Fig. 2d). The AF stations were 10 m tall and were located within the tree strips, except the station at Vechta AF, which was 5 m tall and was located at the crop field (Fig. 2). The OC/OG stations were 3 m (Forst and Mariensee), 3.5 m (Dornburg and Wendhausen) or 5 m tall (Vechta) (Table 6) and were located approximately at the center of the OC/OG sites. The station at Dornburg AF was relocated 10 m in NW direction at the beginning of the second phase of the project in August 2019.

The measurement period varied by region and variable (Table A2). At Dornburg, Forst, and Wendhausen, EC and meteorological measurements were performed from spring 2016 to Autumn 2024, with an interruption from January 2018 to mid 2019. At Mariensee, measurements covered the period from spring of 2016 to the end of 2021, with a similar long gap from January 2018 to mid 2019. At Vechta, measurements covered summer 2019 to autumn 2024. The site-years were considered

https://doi.org/10.5194/essd-2025-440
Preprint. Discussion started: 28 August 2025

Open Access Earth System Science Data Discussions

110 accounting for all years covered by the measurements, from approximately mid 2016 (all regions except Vechta) or mid 2019 (Vechta) until end of 2021 (Mariensee) or end of 2024 (all the other regions).

Figure 2. Satellite view of the sites, including the distribution of the agroforestry (AF, pink dotted line) and the open cropland or grassland (OC/OG, black dotted line) areas, the location of the eddy covariance stations (dark blue diamond for AF and orange circle for OC/OG), and the footprint climatology derived for the whole measurement period, for AF (dark blue solid line) and OC/OG (orange solid line), for all sites (a-Dornburg, b-Forst, c-Mariensee, d-Vechta, e-Wendhausen). The footprint climatology displayed in the maps corresponds to the 80 % contribution to the footprint. The footprint was calculated using the model of Kljun et al. (2015) in its Python version. Figure created with QGIS v. 3.22.11, aerial map by Google Satellite Maps. © Google 2024.

https://doi.org/10.5194/essd-2025-440
Preprint. Discussion started: 28 August 2025

2.2 Meteorological measurements

The meteorological and turbulence variables (Table 2) measured at the sites are named in accordance with FLUXNET standards (https://fluxnet.org/data/ aboutdata/data-variables/, last accessed 23/01/2025). All the variables were collected at both the AF and OC/OGstations using a similar setup. Atmospheric pressure (*PA*) and photosynthetic active radiation (*PPFD_IN*) were measured only at the AF sites. Air temperature (*TA*) and relative humidity (*RH*) were measured at a height of 2 m at all stations. Shortwave incoming radiation (*SW_IN*), shortwave reflected radiation (*SW_OUT*), long-wave outgoing radiation (*LW_OUT*) and net radiation (*NETRAD*) were measured at a height of 0.5 m below the top of the station (see height in the site description section). *SW_OUT* and *LW_OUT* measurements were only available from 2019 onwards. At Vechta OC, no *LW_OUT* data were available. At Wendhausen OC, the *SW_IN* sensor failed from December 2023 until the end of the project. Atmospheric pressure (*PA*) and precipitation (*P*) were measured at a height of 1 m. *P* at the OC/OG was always taken as the reference because it suffered less from interception, which at the AF was caused by the trees. Soil heat flux (*G*) was measured at all the stations using one soil heat flux plate before 2019 and two plates from 2019 (Table 2) inserted at a depth of 5 cm and randomly distributed. *PPDF_IN* measurements were available from early 2022 in Forst, Dornburg and Vechta, from December 2022 in Wendhausen and not available in Mariensee. *PPFD_IN* was measured at 9.5 m height at the AF sites, next to the other radiation sensors. Data were recorded at a 10 s time step and stored in 30-min files on CR1000X dataloggers (Campbell Scientific, Inc. Logan, UT, USA).

https://doi.org/10.5194/essd-2025-440
Preprint. Discussion started: 28 August 2025

Table 2. Meteorological and turbulence variables measured at the stations and instrumental information. Variable names follow the FLUXNET standards (https://fluxnet.org/data/aboutdata/data-variables/, last access 23/01/2025). The information in this table corresponds to the latest measuring setups. Not all variables were available during the whole project duration. Specifically, the lower-cost eddy covariance setups to measure CO_2 molar density and *RH*, were installed in 2019. From 2016 to 2017, a different setup was used, as described in more detail in Section 2.3 (originally in Markwitz and Siebicke, 2019).

Measured variable	**Units**	**Instrument**	**Model**	**Company**
Precipitation, *P*	mm	Precipitation transmitter	5.4032.35.007	Thies Clima, Göttingen, Germany
Atmospheric pressure, *PA*	kPa	Baro transmitter	3.1157.10.000	Thies Clima, Göttingen, Germany
Net radiation, *NETRAD*	$\mathrm{W\ m^{-2}}$	Net radiometer	NR Lite2	Kipp & Zonen, B.V., Delft, The Netherlands
Shortwave incoming radiation, *SW_IN*	$\mathrm{W\ m^{-2}}$	Pyranometer	CMP3	Kipp & Zonen, B.V., Delft, The Netherlands
Shortwave outgoing radiation, *SW_OUT*	$\mathrm{W\ m^{-2}}$	Pyranometer	CMP3	Kipp & Zonen, B.V., Delft, The Netherlands
Longwave outgoing radiation, *LW_OUT*	$\mathrm{W\ m^{-2}}$	infra-red temperature sensor	IN510	Omega Engineering GmbH?
Photosynthetic Active Radiation, *PPFD_IN*	$\mu\mathrm{mol}_{CO_2}\ \mathrm{m^{-2}s^{-1}}$	PAR sensor	PQS 1	Kipp & Zonen, B.V., Delft, The Netherlands
Relative humidity, *RH*	%	Hygro-thermo transmitter-compact	1.1105.54.160	Thies Clima, Göttingen, Germany
Air temperature, *TA*	°C	Hygro-thermo transmitter-compact	1.1105.54.160	Thies Clima, Göttingen, Germany
CO_2 molar density, LC setup, r_c	$\mu\mathrm{mol}_{\mathrm{CO_2}}\ \mathrm{m_{air}}^{-3}$	Infrared gas analyzer	GMP343	Vaisala Oyj, Helsinki, Finland
RH (from LC setup)	%	Relative humidity cell	HIH-4000	Honey-well, Charlotte, North Carolina, USA
Soil heat flux, *G*	$\mathrm{W\ m^{-2}}$	Soil heat flux plates	HFP01	Hukseflux, Delft, The Netherlands
Wind velocity components, *u*, *v*, *w*	$\mathrm{cm\ s^{-1}}$	Ultrasonic anemometer	uSONIC-3 Omni	METEK GmbH, Elmshorn, Germany

2.2.1 Processing of meteorological data

Meteorological measurements were filtered to remove outliers, based on a plausibility range for all variables, and resampled to a time resolution of 30 min to match the time resolution of the EC time series. All the measurements were averaged from 10 s to 30 min resolution, except precipitation, which was summed up over the 30 min period. For all variables, if less than 25 % of the 30 min period values were available, the average or sum corresponding to that variable and that period was marked as a not-a-number (NaN) value. Afterwards, saturated water vapor pressure (e_{sat}) and actual water vapor pressure (e) were obtained following the Magnus-Tetens formulation (Eq. 2 and 3 in Vuichard and Papale, 2015); based on Murray, 1967). Vapor pressure deficit (*VPD*) was calculated as the difference between e_{sat} and e.

2.2.2 Gap-filling of meteorological data

Gaps in the time series of meteorological variables were filled following a four-steps routine. First, very short gaps up to one hour were filled using linear interpolation. This was applied to all variables except *P*. Second, if there were gaps at one station within a region, but the data were available at the paired station, then gaps were filled with linear regression between the two stations. This was applied to all variables except *P*, which was filled by replacing the missing value one by one. In the case of *PA* and *PPFD_IN*, the whole time series were inserted into the OC/OGstations datasets, because these variables were only measured at the AF. Furthermore, at Vechta the missing *LW_OUT* values at the OC station were filled with the measurements at the AF, because the land cover around both AF and OC stations was similar. At Wendhausen, the missing *SW_IN* data from December of 2023 until September 2024 were replaced with the measurements at the AF station.

Third, longer gaps were filled with a similar approach to that employed in FLUXNET (Pastorello et al., 2020; Vuichard and Papale, 2015), with slight differences. ERA5-Land re-analysis data (Muñoz-Sabater et al., 2021) were used as predictor for the missing data, instead of ERA5 re-analysis data (Hersbach et al., 2020) as employed in the FLUXNET central processing pipeline (Pastorello et al., 2020), due to their enhanced spatial resolution of 9 km. The data were requested using the API of the Climate Data Store from Copernicus (https://cds.climate.copernicus.eu/datasets; last accessed 15-11-2024) with the Python library *cdsapi* (https://pypi.org/project/cdsapi/). The ERA5-Land time series of 2 m *TA*, 2 m dew-point temperature (TA_d), *SW_DOWN*, horizontal wind speed South-North direction *WS_N*, horizontal wind speed West-East direction *WS_E* and *PA* were first down-sampled to 30 min time resolution from the original 1 h time step, using linear interpolation. *P* was not interpolated. *WS* and *WD* were calculated by applying basic trigonometry to both horizontal wind speed components. Finally, *RH* and *VPD* were calculated from 2 m *TA* and TA_d, using the same formulation as explained above in section 2.2.1, and the relations between *RH* and *VPD*.

Gaps in *SW_IN*, *PA*, *TA*, *RH*, *VPD*, wind speed (*WS*) and wind direction (*WD*) were filled using linear regressions between the ERA5-Land data and the station data. Despite their high degree of variability at the local scale, *WS* and *WD* were also filled by this procedure because it is difficult to find a set of predictor variables to perform a more sophisticated type of regression (see next paragraph). In the case of *WS*, *WD* and *SW_IN*, the intercept of the linear models was forced to be zero, to exclude the possibility of having negative data as a model result (e.g. a negative *WD* or a negative *SW_IN*), which would not be physically consistent. In the case of the other variables, both slope and intercept were used to generate the new data. Due to its different nature, *P* was gap-filled at the hourly scale by multiplying ERA5-Land data by a factor calculated as the ratio of the total sum of *P* measured at the station and the total sum of *P* from ERA5-Land, for the target period (Vuichard and Papale, 2015). Finally, *PPFD_IN* was filled by multiplying *SW_IN* by a factor obtained as the ratio between measured *PPFD_IN* and *SW_IN*.

https://doi.org/10.5194/essd-2025-440
Preprint. Discussion started: 28 August 2025

The fourth step consisted in a different approach to fill the variables that vary more at the local scale and may not correlate well in general with ERA5 or ERA5-Land re-analysis data. These variables were: *NETRAD*, *LW_OUT*, *SW_OUT* and *G*. This approach used Extreme Gradient Boosting (XGBoost), a machine learning tool belonging to the tree-decision algorithms (Chen and Guestrin, 2016). This algorithm was also applied for gap-filling flux densities (see Section 2.3.2). The code was adapted from the original version published by Vekuri et al. (2023) to gap-fill meteorological data. A more detailed description of the algorithm can be found below, in Section 2.3.2. The predictors used to gap-fill *NETRAD*, *LW_OUT*, *SW_OUT* and *G* were *SW_IN*, *TA*, *VPD* and *PA*, all of them already gap-filled with the linear regressions in the previous step; and *NETRAD* from ERA5-Land data. Due to the nature of XGBoost, the relevance of the different predictors for modeling the target variable is evaluated. Consequently, the incorporation of variables such as *VPD* or *PA* to the set of predictors for, e.g. radiation variables, does not introduce bias in the results (see following Section 2.3.2 for more information).

The gap-filling of completely missing variables (see Table 3), such as *PPFD_IN* before 2022 or *LW_OUT* before 2019, was done by directly applying the steps three and four outlined previously. Therefore the provided time series of these variables are completely modeled before those dates. The accuracy of the gap-filling was considered sufficient due to the good representation of ERA5-Land data of the meteorological conditions at the sites (Fig. B1).

A flag was generated for the meteorological data, named with the suffix "_QC_GF". The flag was 0 for measured data, 1 for interpolated data for short gaps, 2 for data filled using the nearby station, and 3 if ERA5-Land data were used as predictors.

2.2.3 Evaluation of gap-filling of meteorological data

The evaluation of the gap-filling was performed by splitting first the datasets in training (80 %) and test (20 %) datasets. The root mean squared error (RMSE) was calculated on the test dataset after training the model and prior to predicting all missing data (Table B1), for both the variables modeled using linear regressions and XGBoost. As additional justification of the gap-filling method, linear models between measured and ERA5-Land data were calculated before training the models for gap-filling (Table B2). In general, ERA5-Land and measured data correlated well, which allowed us to consider that the gap-filling using the linear models was appropriate. No evaluation was performed for *P* and *PPFD_IN*. A comment on the uncertainties related to gap-filling can be found in section 4.2.2.

https://doi.org/10.5194/essd-2025-440
Preprint. Discussion started: 28 August 2025

Table 3. Percentages of measured (*_m*), post-filtered (*_af*) and filled (*_gf*) data for some of the main variables. No column exists for *TAU_af* or *TAU_gf* because no filters or gap-filling were applied to *TAU*. Measured data for flux densities includes all data that could be calculated from raw data, prior to filtering. Filtered data correspond to data that went through the quality checks. Filled data for flux densities refer to the amount of data that were filled. These values were calculated as the averages across all time series originating from the different *USTAR* filters that were applied (see section 2.3.1). Measured data for meteorological variables refer to all available data after de-spiking the initial raw data (see Section 2.2.1). Filled meteorological data would just be the remaining fraction up to a 100 %.

	H_m	*LE_m*	*FC_m*	*Tau_m*	*H_af*	*LE_af*	*FC_af*	*H_gp*	*LE_gp*	*FC_gp*	*TA*	*SW_IN*	*WS*	*P*	*RH*
Dornburg AF	67.36	59.96	59.96	67.36	46.45	35.56	38.85	53.55	64.44	61.15	66.76	65.41	62.14	70.76	65.03
Dornburg OC	68.36	56.23	56.23	68.36	43.49	31.27	30.82	56.51	68.73	69.18	76.74	77.04	68.59	73.69	76.83
Forst AF	71.4	69.06	69.06	71.4	40.97	36.83	37.63	59.03	63.17	62.37	70.96	71.02	62.34	62.08	71.02
Forst OC	73.15	69.63	69.63	73.15	42.59	37.46	38.51	57.41	62.54	61.49	76.9	76.98	65.7	68.64	76.96
Mariensee AF	61.34	56.92	56.92	61.34	40.02	32.59	35.2	59.98	67.41	64.8	60.6	60.62	54.95	61.01	60.59
Mariensee OG	67.28	63.86	63.86	67.28	34.95	29.43	37.24	65.05	70.57	62.76	72.72	72.72	61.82	72.7	72.72
Vechta AF	67.36	59.96	59.96	67.36	32.03	21.42	28.65	67.97	78.58	71.35	58.8	59.14	53.23	57.81	59.14
Vechta OC	68.36	56.23	56.23	68.36	40.44	36.46	38.57	59.56	63.54	61.43	74.63	74.78	61.54	69.01	74.78
Wendhausen AF	71.4	69.06	69.06	71.4	38.11	31.29	31.0	61.89	68.71	69.0	59.34	59.69	53.42	58.95	59.69
Wendhausen OC	73.15	69.63	69.63	73.15	42.49	27.13	27.32	57.51	72.87	72.68	73.9	73.11	70.53	71.85	74

2.3 Eddy covariance measurements

190 During the first phase of the project, covering the years 2016 to 2017, measurements of three-dimensional wind speed and H_2O concentrations only (Table 2) were taken at all the stations to calculate flux densities of latent heat (*LE*, W m^{-2}), sensible heat (*H*, W m^{-2}) and momentum (*TAU*, kg m^{-2} s^{-1}). The LC-EC setup to measure H_2O was based on a BME280 sensor (Bosch, Germany) as described in Markwitz and Siebicke (2019). For details on data processing, filtering and gap-filling and analysis of the *LE* the reader is referred to Markwitz et al. (2020a). The dataset corresponding to that publication can be found in https://zenodo.org/records/4038399 (Markwitz et al., 2020b). The following data processing and gap-filling sections refer to the eddy covariance measurements from 2019 until 2024.

Following the interruption of 2018, in 2019 the measurement setup changed. The measurements of three-dimensional wind speed continued, but the setup for H_2O measurements was replaced by a setup measuring both CO_2 and H_2O concentrations (Table 2), in order to calculate additionally CO_2 flux densities (*FC*, mu mol m^{-2} s^{-1}).

Three-dimensional wind speed measurements were taken with Metek uSONIC-3 Omni ultrasonic anemometers (METEK GmbH, Elmshorn, Germany). CO_2 and H_2O concentrations were measured with a lower-cost EC (LC-EC) setup, previously prepared at the University of Exeter (Hill et al., 2017). The LC-EC setups consisted of a CO_2 infrared gas analyzer (IRGA) combined with a RH capacitance cell and sensors for temperature and pressure to derive H_2O mole fraction from *RH*. These sensors were isolated within a custom made enclosure. The air was sampled below the sonic anemometer and then directed to the enclosure using Synflex 1300 tubes (1300-M0603, Eaton Corporation, Dublin, Ireland) and across two stainless steel filters with a pore size of 2 μm (SS-4FW-2, Swagelog, Solon, Ohio, USA). The length of the tubes depended on the station height

https://doi.org/10.5194/essd-2025-440
Preprint. Discussion started: 28 August 2025

(9 m at the AF stations, 4.5 m in Vechta AF and OC, and around 2.5 m at the other OC/OG stations). Nominal flow rate was 2.2 L min^{-1} until summer 2022, when pumps were replaced by stronger ones to get a flow rate of 5.0 L min^{-1}. Data from the EC setups were logged at a 2 Hz frequency by CR6 dataloggers (Campbell Scientific, Inc. Logan, UT, USA) in files of 30 min duration. Data from the ultrasonic anemometers were logged additionally at 20 Hz frequency in separated files. The flux density calculation was done using the 2 Hz dataset, however upon request the 20 Hz raw data can be made available from the authors. The LC-EC setups were validated in Callejas-Rodelas et al. (2024) and van Ramshorst et al. (2024). The data from the validation are available in two different repositories which can be found in the corresponding publications. Additional details about the setups, including information about all the sensors of the enclosure and a scheme of the setup, can be found in Callejas-Rodelas et al. (2024).

Both meteorological and eddy covariance measurements were backed up and uploaded to a server using Ethernet connections and Raspberry Pi 2, model B processors (Raspberry Pi Foundation, Cambridge, UK). The stations were solar powered, with the installation comprising monocrystalline solar panels (model 3-01-001245, from Offgridtec GmbH, Eggenfelden, Germany), lithium batteries (type S12/130, code NGS0120130HS0CA, from Exide Technologies GmbH, Büdingen, Germany) and solar charge controllers (model PR 10–30, from KATEK Memmingen GmbH, Memmingen, Germany).

2.3.1 Processing of eddy covariance data

Raw turbulence data were processed using the EddyUH software (Mammarella et al., 2016) in its Matlab version (MATLAB, R2023a). Input meteorological data were *TA*, *RH* and *PA*, which were gap-filled using the nearby station (AF-MC), following steps one and two explained in Section 2.2.2. *FC*, *LE*, *H* and *TAU*, among other relevant parameters, were calculated from the raw data of 2 Hz frequency, by applying the following processing routine. De-spiking of the data was performed by applying absolute difference limits between consecutive data points (Mammarella et al., 2016; Aubinet et al., 2012). Block-averaging for de-trending the data followed the approach explained in Rannik and Vesala (1999). Coordinate rotation for the three-dimensional wind field was carried out through the planar fit method described in Wilczak et al. (2001). Low-frequency losses due to block-averaging and finite period integration were corrected for according to Rannik and Vesala (1999). High-frequency losses due to the low-pass filtering effect of the instruments, especially pronounced due to the use of slow response sensors in the LC-EC setup (Callejas-Rodelas et al., 2024; van Ramshorst et al., 2024), were corrected with the experimental approach of Mammarella et al. (2009). A quality flag depending on the state of turbulence was assigned to all flux density time series, with integer values ranging from 1 to 9 following the approach of Foken et al. (2005). Random uncertainty was estimated according to Finkelstein and Sims (2001). Data were processed on a yearly basis, as recommended by the processing standards of ICOS and FLUXNET (Pastorello et al., 2020; Sabbatini et al., 2018), and in order to ensure a better accuracy of the calculation of the transfer function for H_2O. Exceptions were some periods shorter than one year that were added to the processing of the previous/posterior year. More details on how the transfer functions were calculated can be found in the original paper (Mammarella et al., 2009), and further information on the processing routine for the LC-EC setups is given in (Callejas-Rodelas et al., 2024). When the dependency of H_2O time response with RH could not be estimated accurately, the coefficients of the fit corresponding to the previous year were employed.

https://doi.org/10.5194/essd-2025-440
Preprint. Discussion started: 28 August 2025

After flux density calculations, *FC*, *H* and *LE* were filtered to remove outliers and to ensure a good quality of the measurements. Outliers were removed following the approach of Mauder et al. (2013), based on a median absolute deviation (MAD) filter, since it is a robust outlier detector (Leys et al., 2013). The MAD filter was used for positive and negative values of *FC*, with the threshold parameter q (Eq. 1 in Mauder et al., 2013) being 7.5; for *LE* and *H*, the same approach was applied for positive values, while for negative values, a hard limit of -100 W m^{-2} was applied to *H* and of -20 W m^{-2} to *LE*, rejecting data below that threshold. A moving window of 14 days was used for calculating median and MAD values and for removing outliers, and three iterations were performed on each time series to increase the robustness of the outlier removal. After the MAD filter, additional hard upper and lower limits were applied. These limits were 700 W m^{-2} for *H* and *LE*, and -50 µmol m^{-2} s^{-1} and 40 µmol m^{-2} s^{-1} for *FC*. Only good quality data (e.g. sufficiently well-developed turbulence) according to data quality flags between 1 and 6 were accepted (Foken et al., 2005).

Additionally, *H*, *LE* and *FC* were filtered according to friction velocity values, to ensure a well developed turbulence. The *USTAR* threshold was estimated following the procedure of Papale et al. (2006), based on the method by Reichstein et al. (2005). Following FLUXNET processing pipeline (Pastorello et al., 2020), 40 different *USTAR* thresholds were calculated and applied. The 40 thresholds were withdrawn as the percentiles 2.5% to 97.5%, in steps of 2.5 %, of the distribution of estimated *USTAR* values. *USTAR* thresholds were calculated on a yearly basis. Table 4 shows the averages of *USTAR* thresholds corresponding to the 2.5 % and 97.5 % percentiles, across years. This procedure led to 40 different time series for each variable, i.e. *H*, *LE* and *FC*. The gap-filling (Section 2.3.2) was performed on these time series.

Table 4. Average across years of *USTAR* thresholds corresponding to the percentiles 2.5 % and 97.5 % withdrawn from the distribution of *USTAR* values.

	USTAR_2.5 (m s^{-1})	USTAR_97.5 (m s^{-1})
Dornburg AF	0.17	0.37
Dornburg OC	0.11	0.21
Forst AF	0.14	0.23
Forst OC	0.1	0.16
Mariensee AF	0.16	0.23
Mariensee OG	0.11	0.15
Vechta AF	0.13	0.19
Vechta OC	0.14	0.21
Wendhausen AF	0.19	0.24
Wendhausen OC	0.14	0.2

2.3.2 Gap-filling of eddy covariance data

Gaps in the time series of *FC*, *LE* and *H* were filled using the combination of two methods, as also applied in (Winck et al., 2023). First, the full time series were gap-filled using the Marginal Distribution Sampling (MDS) algorithm (Reichstein et al.,

https://doi.org/10.5194/essd-2025-440
Preprint. Discussion started: 28 August 2025

Earth System Science Data Discussions
Open Access

2005), implemented in REddyProc. The output of REddyProc provides a quality flag depending on the reliability of the filled data, ranging from 0 to 3. Original data have a quality flag of zero. Highly reliable gap-filled data have a quality flag of 1, as these data correspond to short gaps of up to few hours duration with low uncertainty from gap-filling (Wutzler et al., 2018). Data with flags of 0 and 1 were selected after using the MDS algorithm. Later on, the remaining gaps were filled using the XGBoost method. Prior to apply this algorithm, additional hard limits were applied to winter and autumn months to prevent a bias during those periods, due to the large sensitivity of XGBoost to the input data used to train the model. For *H* and *LE*, these hard limits were 100 W m^{-2} in October and March and 50 W m^{-2} from November to February. For *FC*, the hard limits were $\pm$ 10 mu mol m^{-2} s^{-1} from November to February and $\pm$ 15 mu mol m^{-2} s^{-1} in October and March.

The original code implementing XGBoost was used in Vekuri et al. (2023) to fill *FC* flux densities and later on adapted in Callejas-Rodelas et al. (2025a) to gap-fill *H* and *LE* as well, with a different combination of predictors. This later version, from Callejas-Rodelas et al. (2025a), was employed to generate the current datasets. The meteorological drivers used for the gap-filling were *SW_IN*, *TA*, *VPD*, *WS* and *WD*. *WS* was included to consider the effect of a changing fetch area for the flux density measurements, and *WD* was included to account for the heterogeneity across the AF sites and some of the OC/OG sites. The gap-filling was applied separately to all 40 different time series for each variable *H*, *LE* and *FC*.

2.3.3 Implementation of XGBoost

The XGBoost algorithm and other associated functions for the gap-filling were implemented using the Python libraries *xgboost* (Chen and Guestrin, 2016) and *scikit-learn* (Pedregosa et al., 2012). The parameters used in the implementation of XGBoost were kept similar to Vekuri et al. (2023). The time information, directly linked to seasonality in phenology and both seasonality and diurnal variability in meteorological variables, was included as in the original code of Vekuri et al. (2023), by adding to the XGBoost two cyclical functions for month and time of the day and an additional linear description of time. This was valid for the gap-filling of both meteorological and flux density data. The model evaluation was done by calculating the root mean squared error (RMSE) between modeled and measured data, after fitting the model to the training dataset, prior to predicting all missing data. The original code can be found in the repository linked to the publication of Vekuri et al. (2023) (https://github.com/hvekuri/co2_gapfilling, last access: 12 February 2025). The modified version of the code, adapted to the current datasets, can be found in the data repository linked to this publication.

2.3.4 Evaluation of gap-filling and uncertainty estimation of eddy covariance data

The uncertainty due to gap-filling can be evaluated in different ways, depending on how data are aggregated. Errors in individual 30-min data can be assigned using either a reference to another setup or the random error. In the paper by Callejas-Rodelas et al. (2025a), errors in measured data were considered in two distinct manners. In the first case, errors were calculated as the deviation of fluxes between lower-cost and conventional EC setups (Callejas-Rodelas et al. (2024) and van Ramshorst et al. (2024)). This deviation was considered as the worst case RMSE of the linear regression models of *FC* and *LE*, separately. In the second case, errors were calculated as the sum of that deviation and the random error (Callejas-Rodelas et al., 2025a). Errors in gap-filled data with REddyProc were defined as the standard deviation of the data points used for gap-filling (Wutzler et al.,

https://doi.org/10.5194/essd-2025-440
Preprint. Discussion started: 28 August 2025

2018). Finally, the error in gap-filled data with XGBoost was taken as the RMSE between modeled and measured data, after fitting the XGBoost regressor and prior to predicting all missing data, similarly to the meteorological data filled with XGBoost. RMSE values of gap-filled *FC*, *LE* and *H* are displayed in Table 5. The individual errors can be propagated if a cumulative sum is calculated, as explained in Section 2.5 of the paper by Callejas-Rodelas et al. (2025a).

Both REddyProc and XGBoost reproduced the diel cycle of measured data, for *FC* (Fig. C1a) and *LE* (Fig. C1b). The gap-filling led to a reduction of the magnitude of the measured values, due to the fact that most gaps were present during winter and during nighttime, with smaller flux density magnitudes. However, the similarity in diel cycles between measured and filled data can be considered an indicator of reliability of the gap-filling procedure, besides other sensitivity or uncertainty analysis that may be performed.

Table 5. Root mean squared error (RMSE) between modeled and measured data, for *FC*, *LE* and *H*. RMSE was calculated after fitting the XGBoost regressor to measured data and prior to the prediction of all missing data. RMSE was calculated as an average across all 40 *USTAR* scenarios for each variable and site.

	RMSE_FC (mu mol m^{-2} s^{-1})	RMSE_LE (W m^{-2})	RMSE_H (W m^{-2})
Dornburg AF	3.2	27.7	17.3
Dornburg OC	2.5	22.8	10.8
Forst AF	2.4	23.6	13.8
Forst OC	2.2	24.0	11.2
Mariensee AF	2.5	26.2	13.4
Mariensee OG	2.2	25.5	15.0
Vechta AF	3.9	48.8	16.8
Vechta OC	2.5	20.3	11.3
Wendhausen AF	2.8	23.2	14.5
Wendhausen OC	2.8	25.7	14.1

2.4 Partitioning of *FC* into *GPP* and *RECO*

The net ecosystem exchange of CO_2 (*FC*) was partitioned into its photosynthesis (*GPP*) and respiration (*RECO*) components. Both nighttime and daytime models were applied, after Reichstein et al. (2005) and Lasslop et al. (2010), respectively. The partitioning was performed using the REddyProc package in R, version 4.2.1 (Wutzler et al., 2018). The partitioning was applied separately to each of the filled time series of *FC*. This implies the 40 filled *FC* time series led to 80 different final time series of *GPP* and *RECO*, because of the two methods used for partitioning. There was one exception, for Wendhausen OC, where the daytime partitioning method failed and only nighttime *GPP* and *RECO* were provided.

Following Tikkasalo et al. (2025), nighttime *GPP* was forced to zero by subtracting the 1.5 days running median of the nighttime *GPP* from the *GPP* time series and forced any residual nighttime *GPP* to zero. The 1.5 days running median of *GPP*

https://doi.org/10.5194/essd-2025-440
Preprint. Discussion started: 28 August 2025

was then added to the *RECO* time series. This way, the relation *FC* = *RECO* - *GPP* is valid at all time steps and *GPP* is zero when global radiation is zero.

2.5 Flux footprint climatology

The footprint climatology was estimated using the model of Kljun et al. (2015) in its Python version (Python v. 3.6). Separate runs were carried out for the different years at each of the stations, in order to better address the effect of a changing canopy height, and the effect of crop rotation at the different sites. Additionally, a single run with all available data was done, to provide an illustration on the average area measured by the EC stations (Fig. 2). Yearly footprint runs are not shown in the current article, but the results are available at the repository linked to this publication.

The input data to the footprint model were non gap-filled wind data (*WS* and *WD*), roughness length (z_0), *USTAR*, Obukhov length (*MO_LENGTH*), the standard deviation of lateral wind speed (*V_SIGMA*), boundary layer height (*PBLH*, retrieved from ERA5, Hersbach et al., 2023), measurement height (z_m), displacement height (*d*) and aerodynamic canopy height (h_a). The time resolution of all parameters calculated from the eddy covariance measurements was 30 min, therefore *PBLH* was resampled to match this resolution by linearly interpolating the original hourly time series. Only daytime values were used, based on values of *SW_IN* higher than 10 W m^{-2}. Some hard limits were applied to *MO_LENGTH* (values between -30 and +30 m were removed) and z_m-*d* (values below 2.1 m were removed) to avoid errors while running the model. h_a was calculated during neutral conditions (stability parameter $z/L \leq |0.1|$) based on the procedure by Chu et al. (2018). Complete time series of h_a were estimated as described in more detail in van Ramshorst et al. (2025). This allowed for a better representation of the roughness effects of a spatially and temporally varying canopy, therefore it can be considered as a more accurate procedure compared to the use of a single value representing the average canopy height for the whole site for each time step. *d* and z_0 were estimated as 0.1 and 0.6 times the aerodynamic canopy height, following Chu et al. (2018).

Canopy height at the different sites was estimated using some available tree height measurements and pictures taken across the measurement period at the sites. Canopy height is provided as an ancillary parameter in the dataset.

2.6 Shortcomings of the dataset

In some cases there were certain conditions which reduced the accuracy of the eddy covariance measurements. Firstly, at Dornburg AF, the measurements were conducted in the roughness sublayer and below the canopy height of the tree stripes in the footprint during most of the study period. Trees were very close to the height of the EC station in 2018, and higher than it from mid 2020, a problem which was partially mitigated by a clearcut of an area of 30 m around the station in August 2019. Although data followed the same processing routine as the other datasets and were thoroughly quality checked and filtered, the structure of turbulence might have affected their reliability.

Furthermore, the period January 2020 until March of 2021 was missing in Wendhausen OC, and the year 2021 in Dornburg OC presented a very poor quality. These two site-years were discarded in the final dataset, as the gap-filling would become very uncertain.

https://doi.org/10.5194/essd-2025-440
Preprint. Discussion started: 28 August 2025

Table 6. Average of the main parameters used for the footprint model implementation. Measurement height (z_m), canopy height (z), aerodynamic canopy height (h_a) (calculated as described in van Ramshorst et al. 2025), Obukhov length (*MO_LENGTH*), stability parameter (*ZL*), friction velocity (*USTAR*), standard deviation of lateral wind velocity (*V_SIGMA*) and boundary layer height (*PBLH*). Canopy height was estimated from measurements and pictures of the sites. Mean wind speed (*WS*) and wind direction (*WD*), also needed as input to the footprint model, are displayed in Table 7.

	zm (m)	*z* (m)	h_a (m)	*MO_LENGTH* (m)	*ZL* (-)	*USTAR* (m s^{-1})	*V_SIGMA* (m s^{-1})	*PBLH* (m)
Dornburg AF	10	9.75	6.76	-554.78	-0.06	0.49	0.95	595.23
Dornburg OC	3.5	0.56	0.42	-194.14	-0.02	0.34	0.91	595.23
Forst AF	10	3.71	3.18	1599.58	-0.06	0.42	0.99	625.75
Forst OC	3	0.49	0.36	76.75	-0.02	0.31	0.91	625.75
Mariensee AF	10	4.08	5.00	-482.2	-0.06	0.43	1.03	618.76
Mariensee OG	3	0.50	0.78	153.22	-0.02	0.30	0.97	618.76
Vechta AF	5	4.92	2.58	-31.20	-0.032	0.34	0.92	635.60
Vechta OC	5	0.51	1.89	-329.11	-0.03	0.33	0.92	635.60
Wendhausen AF	10	4.75	6.17	126.88	-0.07	0.45	1.04	620.87
Wendhausen OC	3.5	0.80	0.68	-15.04	-0.02	0.33	1.01	620.87

At Vechta AF, there was only one tree stripe, and the station was located within the crops, and not within the tree stripe 2. Therefore, the representativity of this AF site should be considered with care. Furthermore, the EC data from 2022 to 2024 were not included in the final dataset due to the very noisy flux densities.

3 Results

3.1 Meteorological data

SW_IN was similar between AF and OC/OG, with small variations between both systems attributed to changes in cloud cover along the integration periods of 30 minutes (Table 7). *PA* was measured only at the AF site. Variations in *PA* between the AF and OC/OG sites were expected to be insignificant. *TA* was slightly higher at the AF in Dornburg, Mariensee and Vechta, and slightly lower in Wendhausen, while in Forst it was similar at both sites. *RH* was higher at the OC than at the AF, in Dornburg and Forst, and lower at the OC/OG than at the AF in Mariensee, Vechta and Wendhausen. *VPD* was larger at the AF in Dornburg and Forst, and lower in Mariensee, Vechta and Wendhausen. In general, differences in *TA*, *RH* and *VPD* are negligible for the comparison of AF and OC/OG, likely due to the homogeneity in atmospheric conditions for low distant stations. *WS* was larger at the OC in Dornburg, Wendhausen and Vechta, and larger at the AF in Forst and Mariensee. This is attributed to the in general lower tree height at Mariensee AF, therefore the *WS* measured at 10 m height (AF) is larger than at 3 or 3.5 m height (OG). In the case of Forst AF, this was caused by the station being located at a gap within the tree stripe. At the other sites, however, trees were taller, especially in Dornburg and Vechta, than the AF station, leading to a stronger wind-barrier effect and wind

https://doi.org/10.5194/essd-2025-440
Preprint. Discussion started: 28 August 2025

speed reduction. Additionally, in Dornburg the OC site was located on an open elevated slope, leading to stronger winds. *WD* indicated predominant winds from the Northwest for Dornburg AF and OC, Mariensee AF and Wendhausen OC; and from the Southwest for Forst AF and OC, Mariensee OG, Vechta AF and OC and Wendhausen AF. *P* was calculated as an average over all annual sums at both AF and OC/OG, however, the values at the OC/OG are taken as the reference at all the sites because at some of them (Dornburg, Mariensee and Wendhausen) there was an interception effect from the AF tree canopy.

Table 7. Averages of shortwave incoming radiation (*SW_IN*, W m^{-2}), atmospheric pressure (*PA*, kPa), air temperature (*TA*, °C), relative humidity (*RH*, %), vapor pressure deficit (*VPD*, kPa), precipitation (*P*, mm), wind speed (*WS*, m s^{-1}) and wind direction (*WD*, °) for all sites. For *P*, the value was calculated as the average of the annual cumulative sums across the period 1 July 2016 to 1 July 2024, in order to evaluate full year sums and not partial sums due to the start and end of the datasets. For the other variables, the average was the average of all 30 min values across the 9-years period. *WD* is expressed in degrees (°) from the North direction.

	SW_IN (W m^{-2})	*PA* (kPa)	*TA* (°C)	*RH* (%)	*VPD* (hPa)	*WS* (m s^{-1})	*WD* (°)	*P* (mm)
Dornburg AF	141.2	98.1	10.7	79.1	4.0	2.7	308.5	505.4
Dornburg OC	130.7	98.1	10.6	79.2	3.9	3.2	281.4	513.4
Forst AF	136.9	100.7	10.9	79.1	4.3	2.8	255.9	488.9
Forst OC	134.8	100.7	10.9	80.0	4.2	2.4	217.3	470.2
Mariensee AF	127.3	101.0	10.6	83.2	3.3	2.4	299.5	433.1
Mariensee OG	128.0	101.0	10.5	82.7	3.4	1.7	258.0	467.0
Vechta AF	125.0	100.9	11.2	82.5	3.3	1.7	211.6	672.7
Vechta OC	126.3	100.9	11.1	80.8	3.5	2.0	226.8	603.1
Wendhausen AF	130.5	100.4	11.0	80.3	3.9	2.1	257.7	520.3
Wendhausen OC	132.9	100.4	11.2	79.9	4.0	2.3	276.7	536.8

With respect to the time series of meteorological data, the exemplary time series of *SW_IN* and *TA* (Fig. 3a and b) in Forst AF followed a marked seasonality, with the largest values in June for *SW_IN* and July for *TA*, and the lowest values in December for *SW_IN* and in January for *TA*. There was a longer gap in 2019, and additional multiple shorter gaps of few weeks or months in the other years. Gaps were longer in winter due to the solar powered stations, but this did not seem to affect the performance of the gap filling procedure. In the case of *WS*, gaps were longer, especially in 2018 and part of 2019, but the gap-filling seemed to appropriately reproduce the expected variable behavior at the site in terms of seasonal and diurnal variations.

https://doi.org/10.5194/essd-2025-440
Preprint. Discussion started: 28 August 2025

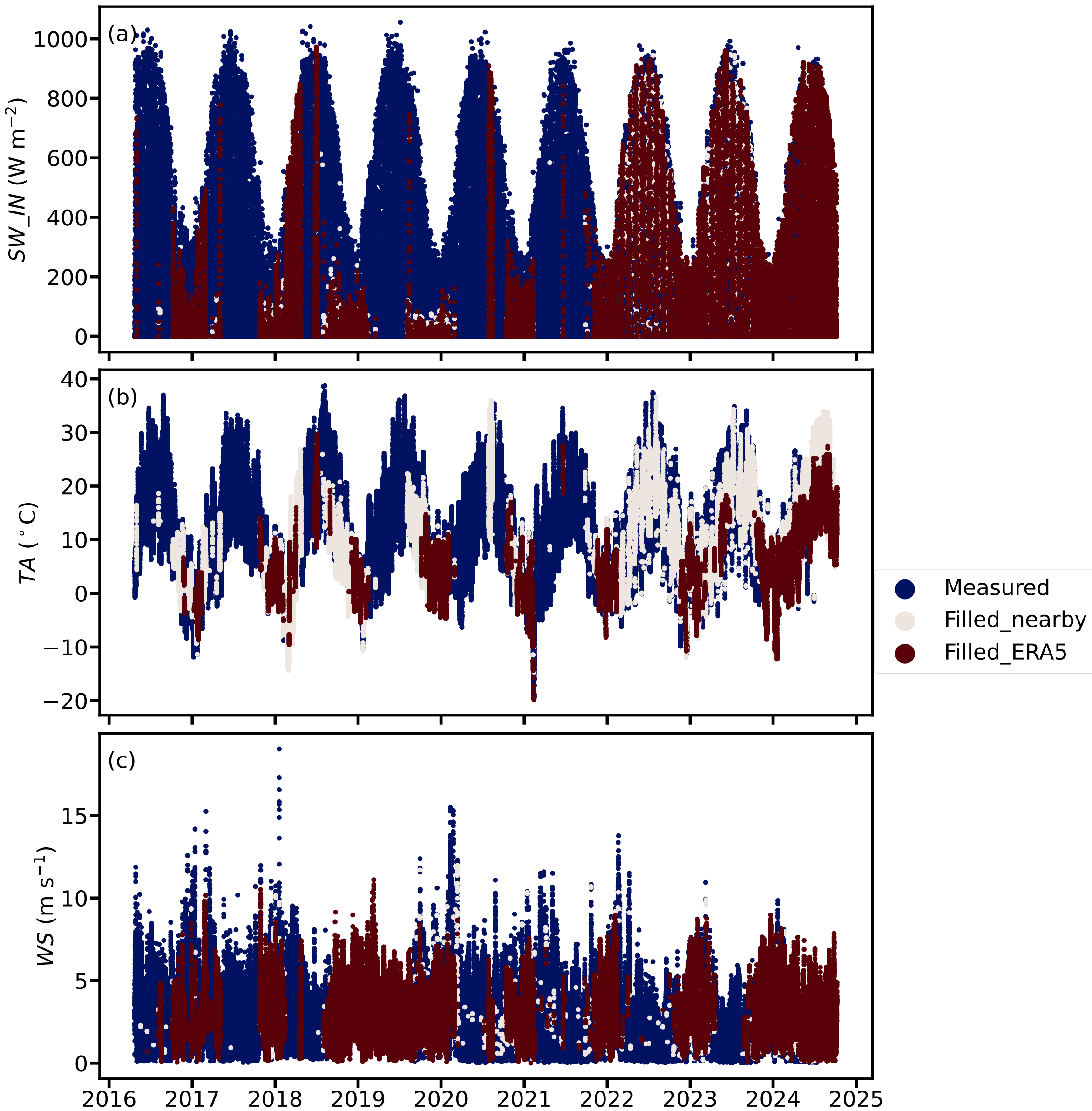

Figure 3. Exemplary time series of shortwave incoming radiation (*SW_IN*, W m^{-2}) (a), air temperature (*TA*, °C) (b) and wind speed (*WS*, m s^{-1}) (c) at Forst AF, at 30 min time resolution. Dark blue markers indicate measured data, light pink markers indicate data filled using either interpolation or the nearby station as a reference, and burgundy markers indicate data filled using ERA5-Land data as a reference (see Section 2.2.2).

The gap-filled data reproduced the seasonality and trends in all variables. In general, the agreement between measured meteorological variables and ERA5-Land data is good (Fig. B1 and Tables B2 and B1), which justifies the use of the gap-filling procedure. For *WS* and *WD*, the correlation between measured and ERA5-Land data is worst and varies more across

https://doi.org/10.5194/essd-2025-440
Preprint. Discussion started: 28 August 2025

sites, which can be explained by locally induced effects on the wind field and to a potential time shift between point data and
375 gridded data (Lipson et al., 2022). For *SW_IN*, slopes are very close to 1.0, but because there is a large scatter in the data (Fig. B1), RMSE is also large. This is caused by locally varying cloud conditions.

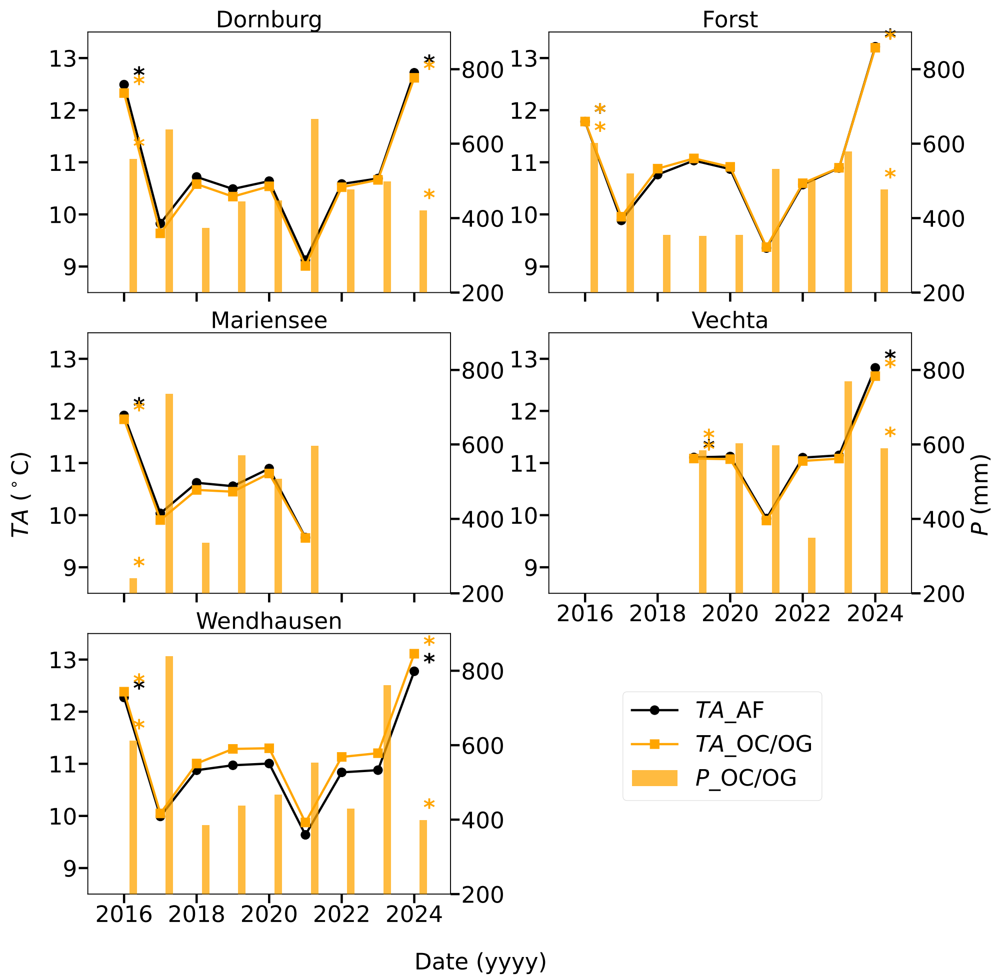

Figure 4. Annual averages of air temperature (*TA*, °C) and annual sums of precipitation (*P*, mm) for all the sites. Black circles with solid line represent the *TA* values at the AF sites. Orange squares with solid line represent the *TA* values at the OC/OG sites. Light orange bars represent annual sums of *P* at the OC/OG sites, taken as a reference for the sites. The measurement period started in spring of 2016 at all sites, except in Vechta, where it started in summer of 2019. Due to this, and due to the incomplete year of 2024 because of the end of the project, the data corresponding to 2016 and 2024 (and 2019 for Vechta), should be considered with care. Data corresponding to incomplete years are marked with asterisks.

Dornburg, Mariensee and Vechta experienced a higher annual *TA* at the AF than at the OC/OG (Fig. 4), while in Wendhausen, *TA* was lower at the AF, and in Forst it was similar for both sites. However, the differences were very small between AF and OC/OG. 2021 was the coldest year at all sites, while the other years were relatively similar. 2016 and 2024 for all sites, and

https://doi.org/10.5194/essd-2025-440
Preprint. Discussion started: 28 August 2025

2019 for Vechta, should not be considered because the average does not comprise some of the coldest months of the year. *P* was largest in Vechta, followed by Wendhausen, and lowest in Forst. 2018 was the driest year at all places, except in Vechta. The driest year in Vechta was 2022. In Forst the annual sum of *P* in 2018 was similar to 2019 and 2020, likely indicating a longer term drought event.

3.2 Eddy covariance flux densities

All flux density time series (for *FC*, *LE* and *H*) at the exemplary Dornburg AF site exhibited a marked seasonality (Fig. 5), with the largest values at the peak of the growing season (around June and July each year) and the lowest values in winter. *FC* indicated an uptake of carbon throughout the growing season, coinciding in time with a larger *LE*, representing water vapor release from the AF system. The lowest values of *FC* were attained in 2019 and in 2023. *H* was the largest in 2023, corresponding to a lower *LE*. Throughout the whole period, *LE* was in general larger than *H*, indicating that water was not a limiting factor, since more energy was employed to evaporate water from the ecosystem, than to heat up the air next to the surface. The gap-filling reproduced satisfactorily the seasonality and in general it did not appear to bias the time series of flux densities. However, XGBoost smoothed the extreme values of the distributions for all variables, as clearly demonstrated by the gap-filled *LE* values, which were never below 0.

Annual sums of *H* were larger at the OC/OG than at the AF in Dornburg, Forst and Mariensee, while they were lower at the OC than at the AF in Vechta and Wendhausen (Fig. 6). Some years, like 2019 in Wendhausen, showed very similar sums of *H*. With respect to annual sums of *ET*, we found larger annual sums at the AF than at the OC/OG in most of the years at most of the sites, with some exceptions, like the year 2020 in Dornburg, the year 2021 in Mariensee, or the year 2024 in Wendhausen. In general, increases in the magnitude of both *H* and *LE* occurred in some years, like in 2020 in Forst, but there is not a clear correlation between both, because the energy partitioning depended on many factors, such as the available net radiation, the crop present at the system and its phenology, and yearly soil and plant water balances. Annual sums of *FC* (Fig. 7) indicated a larger carbon sequestration at the AF than at the OC/OG in all years except 2019 in Dornburg, in all years except 2019 in Forst, 2019 and 2020 in Mariensee and only one year in Wendhausen (2019). A more negative annual sum of *FC* indicates a higher uptake. In the remaining years, either the OC/OG carbon uptake was larger, or both systems showed a positive carbon balance, indicating a carbon release to the atmosphere. With respect to *GPP*, it was larger at the AF than at the OC/OG in all sites, except in Vechta, where it was similar for both AF and OC. For *RECO*, values were larger at the AF than at the OC in Dornburg, Forst and Vechta, while they were similar in Wendhausen, and lower at the AF than at the OG in Mariensee. Generally, the agreement between nighttime and daytime modeled *GPP* and *RECO* was good in the case of Forst and Dornburg. For the other sites, GPP_{NT} and $RECO_{NT}$ were larger than GPP_{DT} and $RECO_{DT}$, respectively.

The balance between gross primary productivity (*GPP*) and ecosystem respiration (*RECO*), explains the differences in the net carbon balance of AF and OC/OG. The AF sites showed a larger *GPP* than the OC/OG sites, but also a larger *RECO*. This is due to an enhanced physiological activity at the AF compared to the OC/OG sites, with larger leaf area index and an extended growing season of trees in comparison to crops. Exceptions were Vechta, were the vegetation surrounding both AF and OC stations was very similar, therefore leading to very similar carbon balances between both sites; and Mariensee, where *RECO*

https://doi.org/10.5194/essd-2025-440
Preprint. Discussion started: 28 August 2025

Open Access Earth System Science Data Discussions

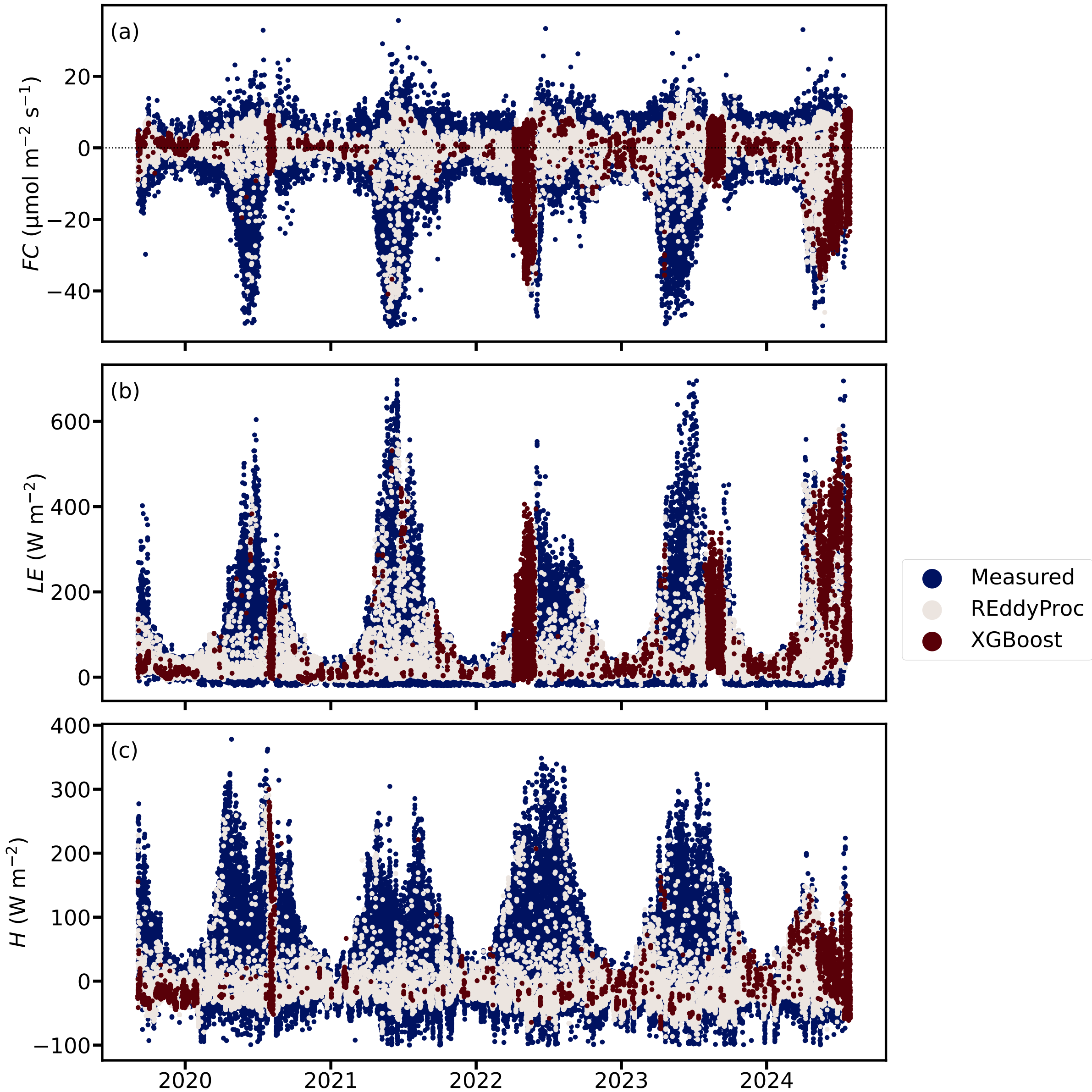

Figure 5. Exemplary time series of flux densities of CO_2 (*FC*, µmol m^{-2}) (a), latent heat (*LE*, W m^{-2}) (b) and sensible heat (*H*, W m^{-2}) (c) corresponding to the 50 % percentile *USTAR* scenario at Dornburg AF. Dark blue markers indicate measured data, light pink markers indicate data filled with REddyProc, and burgundy markers indicate data filled with XGBoost (see Section 2.3.2). The horizontal dashed line in plot (a) represents the 0 uptake line. Negative values of NEE indicate a carbon uptake, while positive values indicate a carbon release.

was larger at the OG because it consisted of low-intensity managed grass. If *GPP* was large due to the presence of the trees
415 at the AF, but *RECO* was also large because there was more biomass respiring and more organic matter being decomposed in

https://doi.org/10.5194/essd-2025-440
Preprint. Discussion started: 28 August 2025

Open Access Earth System Science Data Discussions

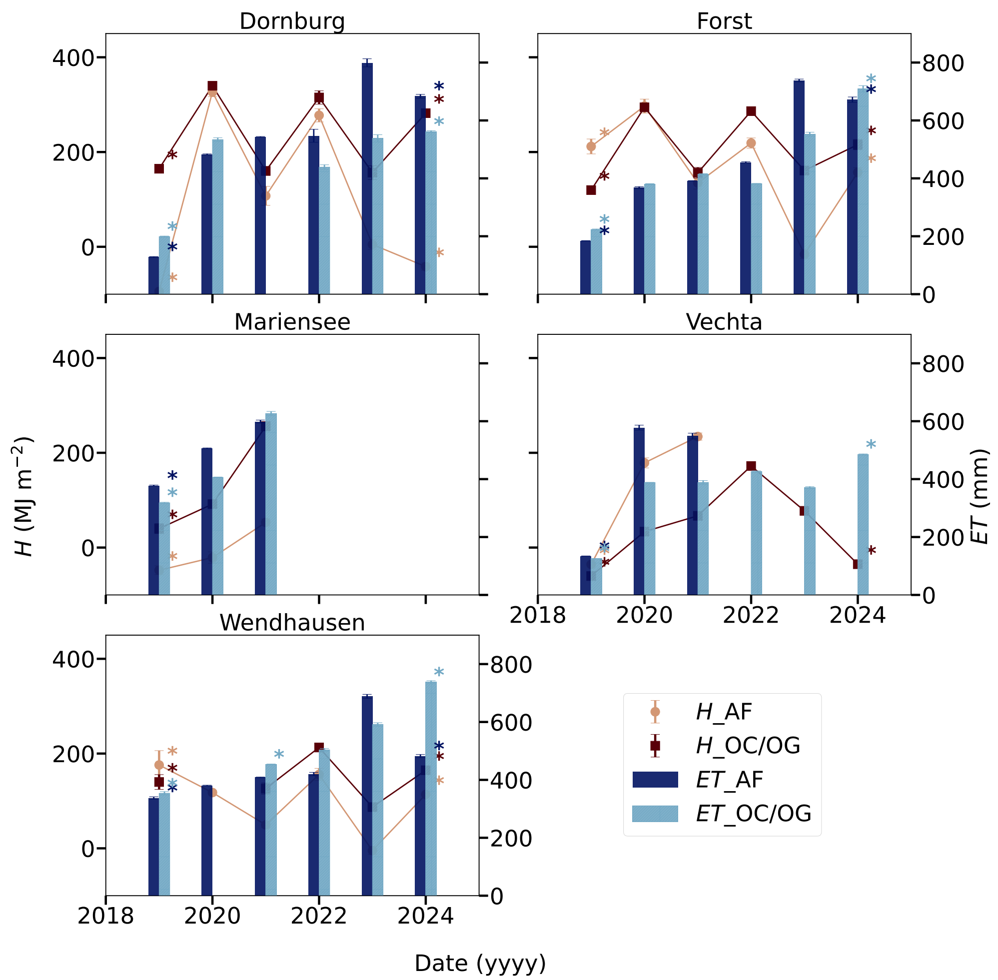

Figure 6. Annual sums of sensible heat flux density (H, MJ m^{-2}) and evapotranspiration (ET, mm) for all the sites. Orange circles with solid line represent the H values at the AF sites. Burgundy squares with solid line represent the H values at the OC/OG sites. Dark blue bars represent the ET values at the AF sites. Turquoise bars represent the ET values at the OC/OG sites. For each annual sum, error bar represents the standard deviation of the sums across all *USTAR* scenarios. The sums corresponding to the years 2019 and 2024 should be considered with care, given that these were incomplete years (see Table A2). The years 2020 in Wendhausen OC and 2021 in Dornburg OC were missing. Additionally, in 2021 the considered period is shorter in Wendhausen OC, because there were three missing months from January to March. Data corresponding to the incomplete years are marked with asterisks.

the soil, then FC would sum for a larger uptake at the OC/OG. In order to evaluate longer term differences, all the individual and year-to-year differences in crops, phenology and climate must be taken into account. Additionally, to assess the overall net carbon balances, carbon export such as the yield and biomass removal from the field after harvest must be taken into account (van Ramshorst et al., 2025). Most values in 2019 were very low, because the growing season was either very advanced or over when the measurements started (Table A2).

https://doi.org/10.5194/essd-2025-440
Preprint. Discussion started: 28 August 2025

Earth System Science Data
Open Access Discussions

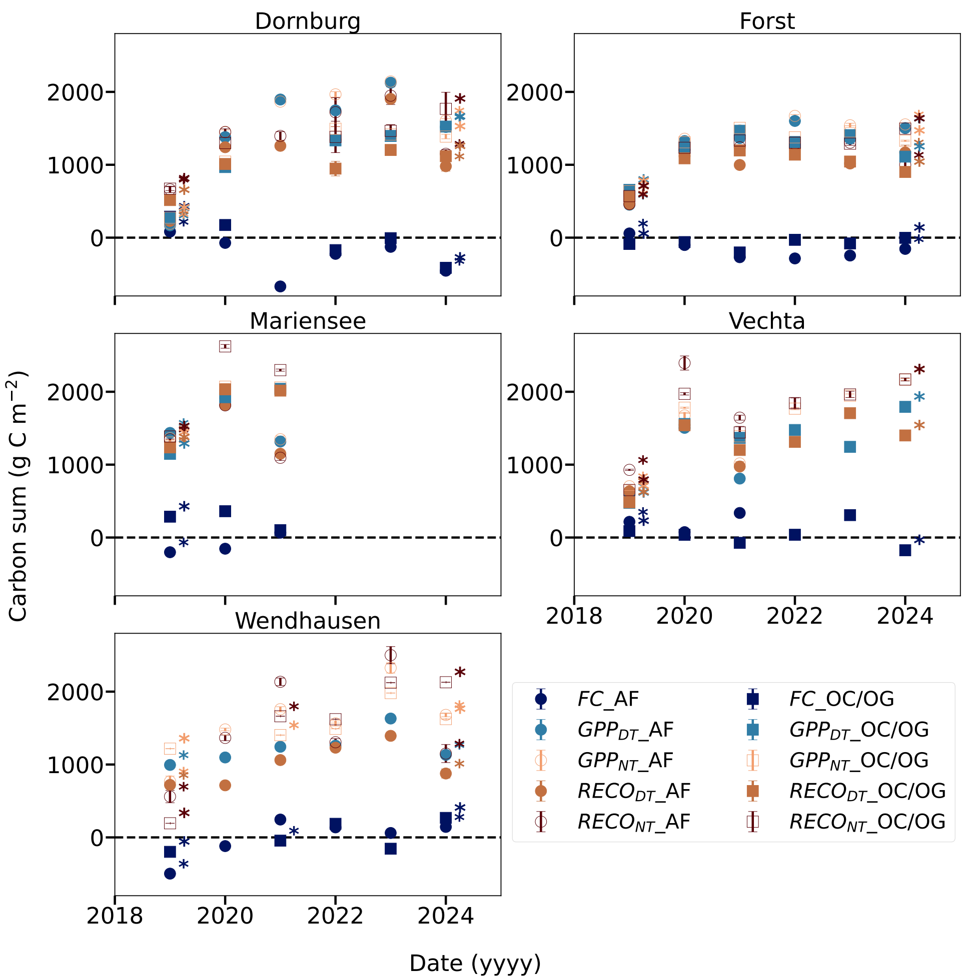

Figure 7. Annual sums of CO_2 flux density (*FC*, g C m^{-2}) (dark blue), gross primary production from the daytime model (GPP_{DT}, g C m^{-2}, solid turquoise markers), gross primary production from the nigthtime model (GPP_{DT}, g C m^{-2}, empty light orange markers), ecosystem respiration from the daytime model ($RECO_{DT}$, g C m^{-2}, solid terracotta markers) and ecosystem respiration from the nighttime model ($RECO_{NT}$, g C m^{-2}, empty red russet markers) for all the sites. Circle markers represent the values at the AF sites. Squared markers represent the values at the OC/OG sites. For each annual sum, error bar represents the standard deviation of the sums across all *USTAR* scenarios. The sums corresponding to the years 2019 and 2024 should be considered with care, given that these were incomplete years. The years 2020 in Wendhausen OC and 2021 in Dornburg OC were missing. Additionally, in 2021 the considered period is shorter in Wendhausen OC, because there were three missing months from January to March. The data corresponding to the incomplete years are marked with asterisks.

https://doi.org/10.5194/essd-2025-440
Preprint. Discussion started: 28 August 2025

4 Discussion

4.1 Novelty and implications of the dataset

The objective of the current publication was to present a harmonized and complete dataset of multiple site-years of meteorological and eddy covariance data over five AF and five OC/OG sites. A total of seventy eight site-years were compiled during this project, which sum up to a consistent dataset that may be re-used by the scientific community. This dataset is unique in its nature, because currently such a comprehensive data set from temperate alley cropping agroforestry systems is not available. In general, harmonized datasets offer the opportunity to study particular phenomena of interest, without the negative sides of data harvesting from different platforms, repositories, personal communications, etc. Datasets focusing on specific ecosystems, which were compiled in order to answer a specific research question, may help to better target and organize further research, by ensuring consistency and alignments in data structure and processing routines.

Particularly, the effect of this type of AF on carbon exchange has not been addressed through EC yet, neither the water use efficiency of both systems, AF and OC/OG, respectively. Furthermore, the dataset can help to understand differences in biophysical effects of the land use change from OC/OG to AF, with implications for the local and potentially global radiative forcing. Based on this data compilation, the modeling of long-term behavior of AF and OC/OG sites, combined with yield modeling through several crop rotations (using complementary data to this publication), could address the question whether this type of AF systems are potentially more resilient to climate change impacts.

Furthermore, the range of studied sites, characterized by distinct crop rotations, soils and climatic conditions, offers the opportunity to examine in detail inter-annual and inter-site variability of the development of a certain crop and its implications on water and carbon balances. The behavior of the AF and OC/OG systems, as a whole, is expected to be different depending not only on the meteorological conditions of a specific season, as well as on the physiology of the crop grown in between the trees, the length of its growing season until harvest, as well as the age of the trees at the AF after tree harvest. The present dataset, complemented by the two years campaign of EC measurements with a distributed network of three EC stations (published in Callejas-Rodelas et al. 2025a), could help to elucidate the discrepancies between AF and OC/OG in carbon and energy balances, as well as on ecosystem properties, depending on the crop type.

Due to the site heterogeneity, particularly at the AF, the footprint model output should be considered with care (Göckede et al., 2004). Nevertheless, the current dataset may help to study the effect of heterogeneity in the AF sites on flux densities, and to test different approaches to better characterize footprints and the source/sink behavior of the areas around the stations. This dataset also provides an opportunity to analyze the effect of canopy heterogeneity, canopy height change and harvest disturbances on the footprint climatology. More refined information on the footprints could be used to assign further quality flags to the flux densities, according to Rebmann et al. (2005) for a more accurate evaluation of carbon and energy exchanges around the stations.

https://doi.org/10.5194/essd-2025-440
Preprint. Discussion started: 28 August 2025

4.2 Uncertainties in the dataset

4.2.1 Uncertainties and errors in the eddy covariance measurements

The uncertainties in the EC measurements from the current datasets are primarily attributable to the inherent characteristics of the EC technique itself, e.g. errors during nighttime measurements and the consequent *USTAR* filtering (Massman and Lee, 2002). Secondly, errors may have arisen from the use of lower-cost eddy covariance setups. Moreover, uncertainty in the measurements may have arose from the station location(Chen et al., 2011). This error may be particularly large above heterogeneous sites such as the AF systems.

The error due to larger spectral corrections in the LC-EC setups (Callejas-Rodelas et al., 2024; van Ramshorst et al., 2024), could be accounted for in different ways. If the goal is to get the strength of carbon and evapotranspiration signals in cumulative sums, the error in individual measurements, in comparison to conventional EC setups, as done in Callejas-Rodelas et al. (2025a) for daily sums, can be used to propagate to an error in the sum using classical error propagation. Another option would be to consider the individual error as the random uncertainty estimated with different methods (e.g. Finkelstein and Sims, 2001; Kessomkiat et al., 2013; Richardson et al., 2008). The measurement error, in comparison to conventional EC setups, could then be propagated together with errors in gap-filled data as explained in section 2.3.4

The study of Callejas-Rodelas et al. (2025a) concluded that the strength of the lower-cost EC setups resides in the fact that they can facilitate replicated measurements, due to their reduced cost. Replicated measurements, especially above heterogeneous ecosystems, allow for a reduction in the error in ecosystem-level balances of carbon and energy (Hill et al., 2017). Furthermore, the higher affordability of LC-EC allows for the deployment of multiple setups at different sites, such as in the current project, therefore providing more datasets and a larger statistical robustness for the research questions.

Finally, with regard to some features of the station location and the footprint size, in Wendhausen AF, Mariensee AF and Vechta AF, the footprint area encompassed most of the target field (Fig. 2), however - under certain conditions - it also extended to some areas beyond it, more marked in the case of Mariensee. This is not shown in Fig. 2, where only the 80 % footprint contour line is displayed. The influence of the areas outside the AF field may be small, but should not be completely neglected when evaluating sources and sinks of carbon and water. For the other sites, the smaller station at the OC/OG sites and the bigger size of the fields in Dornburg AF and Forst AF prevented this effect. In any case, individual year footprints should be considered for a better estimate of the areas measured by the stations, and, only for a qualitative estimate of the distribution of sources and sinks of carbon and water vapor.

4.2.2 Uncertainties in gap-filling meteorological data

The four-step gap-filling procedure applied to meteorological data (Section 2.2.2) enabled to generate consistent datasets with a quality flag indicating gaps filled with linear interpolation, using the nearby station (AF or OC/OG) as a reference, or using ERA5-Land as a reference. In general, if data from a nearby meteorological station are available, the accuracy of using those as a reference is higher than if re-analysis data are used. However, there are inconsistencies in the raw data from the German Weather Service stations close to the field sites, with some missing variables or poor quality data. There are several publications where a number of approaches are applied for gap-filling the main meteorological variables (e.g. Dyukarev, 2023), and some available software packages which facilitate the user application (El Hachimi et al., 2023).

For consistency with FLUXNET datasets, re-analysis data from the European Centre for Medium-Range Weather Forecasts (ECMWF) were used as a reference to fill missing meteorological data. The approach applied in FLUXNET (Pastorello et al., 2020) is based on the original implementation of Vuichard and Papale (2015). Vuichard and Papale (2015) used originally ERA-Interim re-analysis data (Dee et al., 2011) as a reference, but this was updated later on in FLUXNET to use ERA5 data as a reference (Hersbach et al., 2020). Instead, the current datasets were filled using ERA5-Land data as a reference, with improved resolution over the land domain and a better representation of some features, such as orography (Muñoz-Sabater et al., 2021). ERA5-Land data were also used as a reference in Dyukarev (2023) and El Hachimi et al. (2023). It would be advisable to switch the FLUXNET processing routine to a gap-filling procedure which employs ERA5-Land data for terrestrial ecosystem stations. The gap-filling of the meteorological parameters, particularly *TA*, *SW_IN* and *VPD*, is of fundamental relevance for the posterior gap-filling of EC flux densities. Any bias reduction can help reduce the error induced by the gap-filling of EC data.

The gap-filling of most of the variables using linear regression models was considered reliable (Table B1 and Fig. B1) and it was consistent to the FLUXNET implementation, however there was a large scatter in *SW_IN*, *WS* or *WD*. These variables could potentially influence the posterior gap-filling of *FC*, *LE* and *H*. In general, there are unavoidable biases in the match between local point observations, from stations, and grid-scale data, from ERA5 or ERA5-Land (Haiden et al., 2018). This bias could be reduced by employing a more sophisticated approach, such as in Lipson et al. (2022), however it was not implemented in the current dataset. That method improved the correction of ERA5 data to match the local requirements, incorporating a spin-up period for ERA5 data and smoothing hourly biases, and using the logarithmic wind profile to optimize the relation between the ERA5 wind variables and the directly measured variables. This approach would eventually be applicable to any other site.

The gap-filling of the remaining variables (*NETRAD*, *LW_OUT*, *SW_OUT* and *G*), performed with XGBoost, showed a lower RMSE for all variables (Table B1). All variables are radiation or heat transport variables, therefore easier to predict based on other radiation variables or temperature, if compared to ecophysiological variables such as *FC*. Nonetheless, this method was not bench marked against others. In Dyukarev (2023), for example, five different methods were compared to gap-fill the main meteorological parameters, based on all the available parameters of ERA5-Land (a total of 47). This approach, adapted to provide ensemble results (see next section and Lucas-Moffat et al., 2022), could be the solution to obtain more accurate gap-filled meteorological time series, especially for variables with a large site dependency. This could improve posterior flux density gap-filling and a more accurate picture of biophysical ecosystem properties, by providing less uncertain *NETRAD* or *LW_OUT*.

4.2.3 Uncertainties in gap-filling eddy covariance data

The hybrid gap-filling procedure for the eddy covariance data, which combines the MDS algorithm for short gaps and the XGBoost algorithm for the remaining gaps, was selected due to the presence of long gaps in the measured data, and to the demonstrated superior performance of machine learning algorithms compared to the use of only the MDS method (Winck

https://doi.org/10.5194/essd-2025-440
Preprint. Discussion started: 28 August 2025

et al., 2023). Concretely, XGBoost performed better than MDS for filling *FC* over the FLUXNET2015 dataset and for high-latitude sites in Vekuri et al. (2023), and for a long dataset above a deciduous forest in Liu et al. (2025). Due to its handy applicability and the possibility of customizing the predictors and other model parameters, it was chosen as the algorithm to fill longer gaps (of several days up to few weeks or months) for our presented data set. The filled data were carefully examined to check the physical coherence of the values and the seasonality, but some level of uncertainty remained in the datasets, mainly arising from the many missing data (Table 3). This uncertainty may be calculated in different manners, which should be adapted to the specific data aggregation method. A first and easy attempt to estimate the uncertainty in the annual or multiannual sums could be based on individual 30 min errors, as explained in section 2.3.4, or based on the standard deviation across annual balances arising from the different *USTAR* scenarios.

In general, it is desirable that the uncertainty associated to any gap-filling procedure should be of similar magnitude as the noise of the measurements (Moffat et al., 2007). In the current datasets, longer gaps were typically present in winter time. However it was shown in other studies that in temperate or boreal ecosystems, with low physiological activity in winter, long gaps did not add large uncertainty to the data (Richardson and Hollinger, 2007). Moreover, because of having multiple years of data, it was assumed that the gap-filling model could learn appropriately the relations between drivers and flux densities for different times of the year.

The uncertainty in annual balances of *FC* was estimated by Vekuri et al. (2023) and Liu et al. (2025) by creating artificial time series using neural networks and then adding multiple scenarios with different percentages of data coverage. In both studies the authors used XGBoost and compared it to MDS. Based on the error in annual balances from both studies, we could assign an uncertainty in annual sums of *FC* in the current dataset of ± 30 g C m^{-2} from Vekuri et al. (2023), considering the worst case scenario with very long gaps and a small data coverage, and of ± 70 % of the annual sum from Liu et al. (2025) considering the spread across different gap scenarios. The uncertainty in *ET* balances could be considered in a similar manner. We suggest considering these values when making use of the current dataset. More specific analysis, such as the method proposed by Richardson and Hollinger (2007), are planned in future work. Such method allows to disentangle random error and gap uncertainty depending on which time of the year gaps occurred, and focuses on the gap uncertainty rather than the gap-filling method uncertainty.

The EC community is increasingly adopting machine learning algorithms to fill gaps in time series (Lucarini et al., 2024) and there is a number of studies demonstrating their reliability (e.g., Mahabbati et al., 2021, Tramontana et al., 2016 or Zhu et al., 2022). Providing ensemble results from different methods, as recommended by (Lucas-Moffat et al., 2022) and implemented by e.g. Tikkasalo et al. (2025), may solve partially the question of gap-filling method uncertainty. However, machine learning methods are not yet standardized neither used in the processing pipelines of international networks such as FLUXNET (Pastorello et al., 2020) or ICOS (Sabbatini et al., 2018). It is recommended and expected to see more efforts in this direction within the EC community.

https://doi.org/10.5194/essd-2025-440
Preprint. Discussion started: 28 August 2025

4.3 Compare processing routines to FLUXNET

The development of international networks of EC stations, such as ICOS or FLUXNET, aimed to standardize measurements and data processing pipelines with centralized processing protocols and units to increase inter-comparability and reliability of results (Rebmann et al., 2018; Sabbatini et al., 2018). However, the datasets uploaded through a network get embedded in a larger scale processing scheme that may mask site individual features that are relevant for the data to be interpreted or processed. Many EC stations, however, do not belong to these networks, due to the lack of certain measurements, the use of different instruments such as lower-cost setups, or the use of different processing schemes (Pastorello et al., 2020). It is thus important for the EC community that these original datasets are published along with a detailed site characterization and methodological explanation. This was the main motivation for the current publication.

The EC setups deployed within the SIGNAL project do not meet all the standards of FLUXNET in terms of the minimum requirements of instruments and measured variables. The major difference is the use of slow-response gas analyzers for measuring CO_2 molar density and for *RH* measurements, from which later on H_2O mole fraction is derived. The gas analyzers used by the community are capable to sample at higher frequencies, and specifically the analyzer recommended in ICOS is the LI-7200 (LI-COR Inc., Lincoln, NE, USA) (Rebmann et al., 2018; Sabbatini et al., 2018). Regarding the post-processing, applied after the calculation of half-hour flux densities, there were several differences to FLUXNET, from which only the most relevant are pointed out.

Firstly, from the required data variables for post-processing ("Critical data variables for the post-processing, averaged or integrated over 30 or 60 minutes", in Pastorello et al., 2020), in the current datasets the storage of CO_2 (*SC*), the soil temperature (*TS*) and the soil water content (*SWC*) are missing. Compared to the variables in Table 2 of Pastorello et al. (2020), *TS*, *SWC*, outgoing photosynthetic photon flux density (*PPFD_OUT*), diffuse incoming photosynthetic photon flux density (*PPFD_IN*) and diffuse incoming global radiation (*SW_DIF*) are missing inside this work. Additionally, the net ecosystem exchange (*NEE*) is just *FC* in the current dataset because no storage correction was done. With respect to gap-filling meteorological data, for the current dataset ERA5-Land data were used as a reference, instead of ERA5 as in FLUXNET (Pastorello et al., 2020). We included a more advanced approach for some energy and radiation variables which can be important to interpret ecosystem functioning and its biophysical properties. Thirdly, in FLUXNET the gap-filling of *FC*, *LE* and *H* is performed fully using the MDS algorithm, based on Reichstein et al. (2005), whereas the hybrid approach combining MDS and XGBoost was employed for this dataset. Then, the energy balance closure is estimated using three different methods and the corrected *H* and *LE* are provided as an ancillary data product (Pastorello et al., 2020), while in the current datasets no energy balance correction was applied. Regarding *USTAR* filtering, the bootstrapping of the *USTAR* distribution is slightly different in FLUXNET than applied in REddyProc (Wutzler et al., 2018). In FLUXNET, the method of Reichstein et al. (2005), implemented in Papale et al. (2006), was complemented by the change-point detection method after Barr et al. (2013). During the preparation of the current dataset, only the moving point detection method of Papale et al. (2006) was implemented. Thereafter, the use of 40 different *USTAR* thresholds to generate 40 different time series of the flux density variables is similar as in FLUXNET in the case of *FC*, but it is not implemented for *H* and *LE*. A third method implemented in FLUXNET, the sundown partitioning method after van

https://doi.org/10.5194/essd-2025-440
Preprint. Discussion started: 28 August 2025

Gorsel et al. (2009), was not applied to the current dataset because there were no storage data, required by the method. Finally, the partitioning of *FC* into *GPP* and *RECO* was done for both daytime and nighttime based methods, as in FLUXNET, but the time series were forced to fulfill the relation *FC* = *RECO* - *GPP* as explained in section 2.4. This correction is not implemented in FLUXNET.

5 Data records and usage of the dataset

Upon appropriate citation and referencing, users are encouraged to download and work with the current dataset and to reuse the codes, to perform further data analysis, modeling or test of gap-filling algorithms, footprint models, etc. There is a metadata excel sheet in the repository with name, units and description of all the published variables. There are three files corresponding to each station, containing meteorological data at 30-min resolution, except precipitation; eddy covariance data at 30-min resolution; and precipitation data at 1-hour resolution. Missing data are marked with -9999 for original variables. Time coordinate is UTC. Time stamp is 30 min, with the ISO format yyyymmddHHMMSS, and corresponds to the end of the averaging period. Time stamp and variable names follow FLUXNET standards. Year ("YEAR"), day of year ("DOY"), and hour ("HOUR"), are also provided. Additionally, the yearly footprints and the single footprint including all years are published in files, containing the contour lines of the 70, 80 and 90 % contribution to the footprints. The contour lines are defined by "X_" and "Y_" coordinates in EPSG:4326 (WGS84), together with the latitude and longitude coordinates in the coordinate reference system EPSG:25832. The files are named as 'footprint_year_station_contribution%' for the different years and % of footprint contribution, and 'station_contribution' for the single footprint run.

Variable names and units are stored in the file called "variable_name_unit_meteo.csv" and "variable_name_unit_eddycov" for meteorological and eddy covariance data, respectively. The filled time series of *H*, *LE* and *FC* are named as 'variable_name_Uperc_f'. The quality flag columns of the filled data are named as 'variable_name_Uperc_QC_GF'. Time series of *GPP* and *RECO* are named as 'GPP_DT_Uperc', 'GPP_NT_Uperc', 'RECO_DT_Uperc' and 'RECO_DT_Uperc', for daytime and nigthtime modelled *GPP* and *RECO*, respectively. The uncertainty from REddyProc gap-filling is included in the columns 'FC_Uperc_fsd'. 'perc' refers to the *USTAR* percentile, from 2.5 to 97.5 %, in steps of 2.5 %. The original flux density variables, prior to filtering, are named as *FC_ORIG*, *LE_ORIG* and *H_ORIG*. Random error corresponding to these variables is named as *RE.FC*, *RE.LE* and *RE.H*, respectively. Quality flags are named as *FC_QC*, *LE_QC* and *H_QC*, respectively.

All the information that was considered relevant for the interpretation and further analysis of the current dataset was included in this publication or can be found in the files in the linked repository. However, the authors might have missed some details or might not be aware of some features of the sites, which could eventually be important to perform some specific analysis. The users of the dataset are therefore encouraged to contact the authors if missing information is required.

https://doi.org/10.5194/essd-2025-440
Preprint. Discussion started: 28 August 2025

Open Access Earth System Science Data Discussions

6 Code and data availability

615 Data presented in this article can be accessed through https://doi.org/10.25625/A2Z8T8 (Callejas Rodelas et al., 2025b), under a Creative Commons Attribution licence (CC BY-4.0). Codes used to filter, gap-fill, create the figures and extract relevant information for the paper, can be accessed through https://github.com/jangelcrgot/Processing_dataset_multiyear_eddycov_agroforestry, under a GNU General Public License version 3.0 (GPL-3.0). Raw meteorological and eddy covariance data can be provided by the authors upon request.

620 Appendix A: Supporting information on the sites

Table A1. Sowing and harvest dates of crops, harvest dates of trees, and cutting dates for the grassland in Mariensee, throughout the project duration. No precise dates were available for the grass cut in Mariensee, but it was always taking place at late spring (Langhof and Swieter, 2024). In 2023, clover did not grow well in Forst due to the very wet winter conditions, therefore no harvest took place. In 2024, part of the winter wheat in Dornburg was infested by snails and it was replaced in March by summer barley. Harvest of both crops took place on the same day. In Wendhausen, there were three crops, typically summer barley, corn and winter rapeseed, rotating each year across the site. In the table, only the crop located in the main footprint area of the EC station is written down.

	Site Year	Dornburg	Forst	Mariensee	Vechta	Wendhausen
Crop/ sowing-harvest date	2016	Summer barley 25 March - 15 August	Winter wheat 4 November 2015 - 25 August	Grass Late spring	-	Winter rapeseed 8 September 2015 - 20 July
	2017	Winter rapeseed 28 August 2016 - 17 August	Winter barley 22 September 2016 - 21 July	Grass Late spring	-	Winter wheat 27 September 2016 - 7 August
	2018	Winter wheat 16 October 2017 - 27 July	Silo maize 4 May - 3 September	Grass Late spring	-	Winter wheat 18 October 2017 - 18 July
	2019	Summer barley 5 March - 22 July	Summer barley 25 March - 25 July	Grass 23 June	Silo maize 3 May - 20 September	Silo maize 18 April - 23 October
	2020	Summer barley 28 March - 12 August	Bristle oat 17 March - 31 July	Grass 19 June	Winter rye 3 October 2019 - 6 August	Silo maize 21 April - 28 September
	2021	Winter wheat 28 October 2020 - 21 August	Winter wheat 13 October 2020 - 15 August	Grass 16 August	Potatoe 9 April - 20 October	Summer barley 29 March - 30 July
	2022	Winter barley 2 October 2021 - 15 August	Winter barley 24 September 2021 - 4 July	-	Winter rye 3 November 2021 - 28 July	Winter rapeseed 8 September 2021 - 14 July
	2023	Winter rapeseed October 2022 - 11 August	Clover Bad growth	-	Winter rapeseed 3 November 2022 - 20 July	Silo maize 26 April - 26 September
	2024	Winter wheat October 2023 - 13 August Summer barley March 2024 - 13 August	Winter wheat 30 October 2023 - 17 July	-	Rye 9 September 2023 - 01 August	Silo maize 24 April - 13 September
Tree harvest		-	February 2021	February 2021	-	February 2021

https://doi.org/10.5194/essd-2025-440
Preprint. Discussion started: 28 August 2025

Open Access Earth System Science Data Discussions

Table A2. Measurement period for all stations. During the first phase of the SIGNAL project a different EC setup was running at all sites in addition to the meteorological sensors (more details in Markwitz et al., 2020a; Markwitz and Siebicke, 2019). In the table, only the starting dates of the EC setups measuring during the second and third phases of the project are displayed. The EC setup in Vechta AF was removed some months before the end of the project, but the meteorological sensors were still measuring until October 2024.

		Meteorological data	**EC data**
Dornburg	AF	22 April 2016 - 17 July 2024	04 September 2019 - 17 July 2024
	OC	21 April 2016 - 09 October 2024	02 July 2019 - 09 October 2024
Forst	AF	11 March 2016 - 29 August 2024	03 July 2019 - 29 August 2024
	OC	09 March 2016 - 10 October 2024	26 June 2019 - 10 October 2024
Mariensee	AF	17 March 2016 - 29 December 2021	17 May 2019 - 29 December 2021
	OG	17 March 2016 - 31 December 2021	17 May 2019 - 31 December 2021
Vechta	AF	31 July 2019 - 29 August 2024	31 July 2019 - 31 December 2021
	OC	31 July 2019 - 02 October 2024	31 July 2019 - 02 October 2024
Wendhausen	AF	22 March 2016 - 18 September 2024	25 May 2019 - 18 September 2024
	OC	23 March 2016 - 18 September 2024	30 May 2019 - 18 September 2024

Appendix B: Evaluation of gap-filling of meteorological data

Table B1. Root mean squared error (RMSE) for evaluation of the gap-filling of meteorological data. RMSE was calculated between measured and ERA5-Land data in the case of *SW_IN*, *PA*, *TA*, *RH*, *VPD*, *WS* and *WD*, for the test dataset using a 0.8:0.2 ratio of training to test data. RMSE was calculated between predicted and measured data, after model fitting and prior to predicting all missing data, for *SW_OUT*, *NETRAD*, *LW_OUT* and *G*. In this case, RMSE was calculated as the average RMSE of the modeled data for the different split data sets in training and test data, for each variable. More details about the gap-filling can be found in Sections 2.2.2 and 2.3.2.

	SW_IN (w m^{2})	PA (kPa)	TA (°C)	RH (%)	VPD (kPa)	WS (m s^{-1})	WD (°)	SW_OUT (W m^{-2})	NETRAD (W m^{-2})	LW_OUT (W m^{-2})	G (W m^{-2})
Dornburg AF	103.6	3.9	2.1	9.1	0.3	1.1	191.6	12.7	44.5	10.2	6.0
Dornburg OC	109.4	3.8	1.7	9.4	0.2	1.1	192.7	10.0	33.2	8.4	10.0
Forst AF	101.4	0.9	2.0	9.5	0.2	1.0	172.1	7.4	28.4	11.0	7.8
Forst OC	97.5	0.9	1.9	9.1	0.2	1.0	180.4	7.4	22.7	8.1	13.2
Mariensee AF	103.9	1.0	2.1	9.5	0.2	0.9	178.2	7.6	25.0	19.4	3.9
Mariensee OG	94.8	1.0	2.0	9.7	0.2	0.8	166.0	5.5	26.2	37.2	3.8
Vechta AF	98.2	0.5	1.3	7.3	0.2	0.9	176.8	8.4	26.6	7.5	10.1
Vechta OC	93.1	0.5	1.3	7.0	0.2	1.0	169.0	7.3	19.9	7.8	10.9
Wendhausen AF	101.5	1.1	1.8	9.2	0.2	0.9	174.9	9.0	33.7	14.2	8.4
Wendhausen OC	101.5	1.1	1.7	8.9	0.2	1.1	182.9	8.6	21.8	14.7	12.0

https://doi.org/10.5194/essd-2025-440
Preprint. Discussion started: 28 August 2025

Open Access Earth System Science Data Discussions

Table B2. Slopes (a) and coefficients of determination (r^2) of linear regression models (of the form $y = ax + b$) between measured and ERA5-Land data, for *SW_IN*, *PA*, *TA*, *RH*, *VPD*, *WS* and *WD*. The intercept b was forced to be 0 in the case of *SW_IN*, *WS* and *WS*. More details about the gap-filling can be found in Sections 2.2.2 and 2.3.2.

	SW_IN	*PA*	*TA*	*RH*	*VPD*	*WS*	*WD*
Dornburg AF	a = 1.1 r^2 = 0.9	a = 1.0 r^2 = 0.8	a = 1.0 r^2 = 0.9	a = 1.1 r^2 = 0.8	a = 1.1 r^2 = 0.8	a = 1.0 r^2 = 0.9	a = 1.0 r^2 = 0.4
Dornburg OC	a = 1.0 r^2 = 0.9	a = 1.0 r^2 = 0.8	a = 1.0 r^2 = 1.0	a = 1.1 r^2 = 0.7	a = 1.0 r^2 = 0.9	a = 1.2 r^2 = 0.9	a = 1.0 r^2 = 0.3
Forst AF	a = 1.1 r^2 = 0.9	a = 1.0 r^2 = 1.0	a = 1.1 r^2 = 1.1	a = 1.1 r^2 = 0.8	a = 1.1 r^2 = 0.9	a = 1.0 r^2 = 0.9	a = 0.8 r^2 = 0.4
Forst OC	a = 1.1 r^2 = 0.9	a = 1.0 r^2 = 1.0	a = 1.0 r^2 = 1.1	a = 1.1 r^2 = 0.8	a = 1.1 r^2 = 0.8	a = 0.9 r^2 = 0.9	a = 0.8 r^2 = 0.4
Mariensee AF	a = 1.0 r^2 = 0.9	a = 1.0 r^2 = 1.0	a = 1.1 r^2 = 0.9	a = 1.1 r^2 = 0.7	a = 1.1 r^2 = 0.8	a = 0.8 r^2 = 0.9	a = 0.9 r^2 = 0.4
Mariensee OG	a = 1.1 r^2 = 0.9	a = 1.0 r^2 = 1.0	a = 1.0 r^2 = 0.9	a = 1.1 r^2 = 0.7	a = 1.1 r^2 = 0.8	a = 0.6 r^2 = 0.9	a = 0.8 r^2 = 0.4
Vechta AF	a = 1.0 r^2 = 0.9	a = 1.0 r^2 = 1.0	a = 1.1 r^2 = 1.1	a = 1.2 r^2 = 0.8	a = 1.2 r^2 = 0.9	a = 0.8 r^2 = 0.8	a = 0.9 r^2 = 0.4
Vechta OC	a = 1.1 r^2 = 0.9	a = 1.0 r^2 = 1.0	a = 1.0 r^2 = 1.0	a = 1.1 r^2 = 0.8	a = 1.2 r^2 = 0.9	a = 0.7 r^2 = 0.8	a = 0.8 r^2 = 0.3
Wendhausen AF	a = 1.0 r^2 = 0.9	a = 1.0 r^2 = 1.0	a = 1.1 r^2 = 1.0	a = 1.2 r^2 = 0.8	a = 1.2 r^2 = 0.9	a = 0.8 r^2 = 0.9	a = 0.9 r^2 = 0.4
Wendhausen OC	a = 1.1 r^2 = 0.9	a = 1.0 r^2 = 1.0	a = 1.1 r^2 = 1.1	a = 1.2 r^2 = 0.8	a = 1.2 r^2 = 0.9	a = 0.9 r^2 = 0.8	a = 0.9 r^2 = 0.4

https://doi.org/10.5194/essd-2025-440
Preprint. Discussion started: 28 August 2025

Open Access Earth System Science Data Discussions

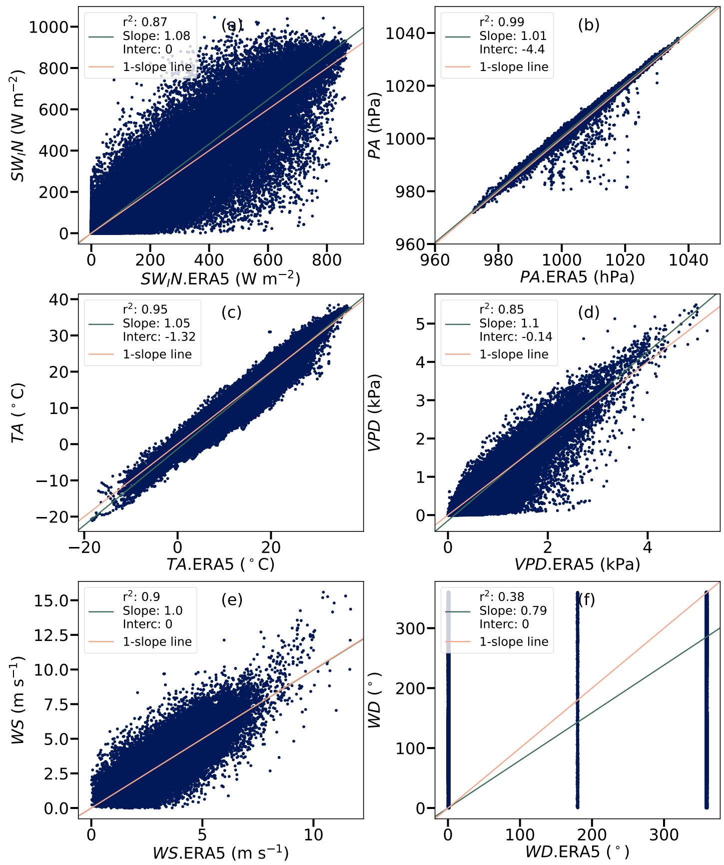

Figure B1. Scatter plots and linear regressions of measured meteorological vs. ERA5-Land re-analysis data, for global radiation (*SW_IN*, a), atmospheric pressure (*PA*, b), air temperature (*TA*, c), vapor pressure deficit (*VPD*, d), wind speed (*WS*, e) and wind direction (*WD*, f), at Forst AF. Data are at 30-min time resolution. The turquoise lines represent the linear regression models between ERA5-Land and measured data, and the pink/orange lines represent the reference 1-slope line with an intercept at 0.0. Slopes, r^2 coefficients and intercepts of the linear models between ERA5-Land and measured data are displayed in the legends.

https://doi.org/10.5194/essd-2025-440
Preprint. Discussion started: 28 August 2025

Open Access Earth System Science Data Discussions

Appendix C: Diel cycles of measured and gap-filled *FC* and *LE*

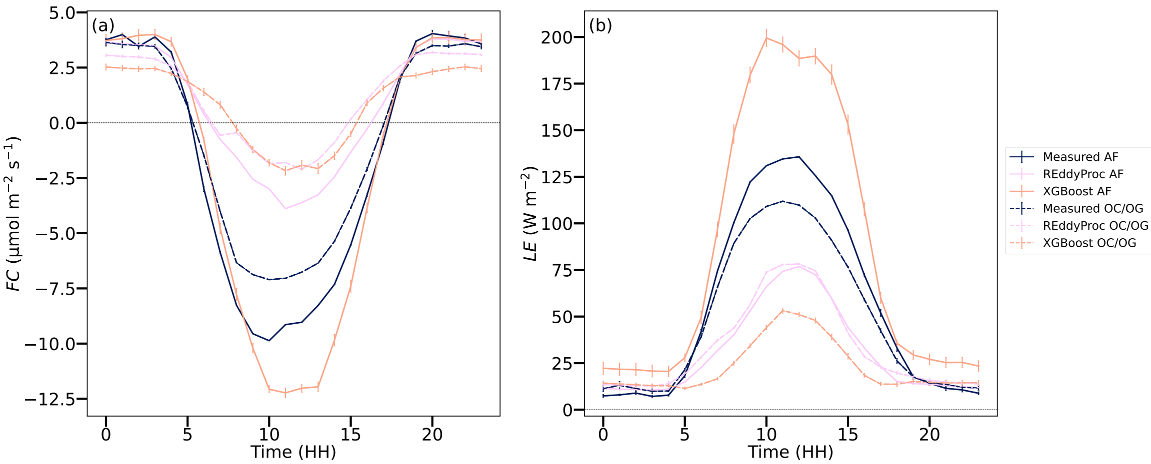

Figure C1. Exemplary mean diel cycle of CO_2 flux density (*FC*, µmol m $^{-2}$ s $^{-1}$) and latent heat flux density (*LE*, W m^{-2}) at Dornburg. Values were calculated as the mean across all available data corresponding to each 30 min period, across all *USTAR* scenarios. Error bars represent the standard deviations over the 40 *USTAR* scenarios. Solid lines represent the AF values, dashed lines represent the OC values. Dark blue colour represents measured data, pink colour represents measured data plus data filled with REddyProc, and light orange colour represents measured data and gap-filled data with both REddyProc and XGBoost. It is important to note that because most gaps occurred in winter and nighttime, the filled data have a different distribution and thus lower magnitude.

Author contributions. JACR, JvR and CM performed field measurements and data analysis during phases III, II and I of the SIGNAL project, respectively. JACR compiled and processed the longer term dataset and wrote the manuscript. JvR contributed to data processing and manuscript writing. AK, LS and CM wrote the project proposal and contributed to data processing and manuscript writing. DF, MP and DB contributed to data collection through technical support during fieldwork.

Competing interests. The authors declare that they have no known competing financial interests or personal relationships that could have appeared to influence the work reported in this paper.

Acknowledgements. We wish to acknowledge the funding agencies for providing the necessary funds to conduct this research, as well as the technical support in the field work received by Frank Tiedemann, Edgar Tunsch and student assistants (Bioclimatology group), and Julian

Meyer (Soil Science group of Tropical and Subtropical Ecosystems) from the University of Göttingen. Further, we wish to acknowledge the contributions by Mathias Herbst to the BonaRes SIGNAL proposal and project design, the support from the team of the Micrometeorology Group at the University of Helsinki and from the Natural Resources Institute Finland (LUKE) in Helsinki, and the preparation of the lower-cost eddy covariance systems by Robert Clement and Timothy Hill from the University of Exeter. We used the library *cmcrameri* in Python to generate figures with color palettes proven to be suitable for people with color vision deficiencies, for which we acknowledge Crameri et al. (2020).

Financial support. This research was supported by the German Federal Ministry of Education and Research (BMBF, project BonaRes, Module A, SIGNAL 031A562A, 031B0510A and 031B1063A) and the Deutsche Forschungsgemeinschaft (grant No. INST 186/1118-1 FUGG). This project also received funding from the European Unions´ Horizon 2020 research and innovation program under Grant Agreement No. 862695 EJP SOIL, the German Academic Exchange Service (DAAD), and the Reinhard-Süring-Foundation (RSS), affiliated to the German Meteorological Society (DMG).

https://doi.org/10.5194/essd-2025-440
Preprint. Discussion started: 28 August 2025

References

Aubinet, M., Feigenwinter, C., Heinesch, B., Laffineur, Q., Papale, D., Reichstein, M., Rinne, J., and Van Gorsel, E.: Nighttime Flux Correction, in: Eddy Covariance: A Practical Guide to Measurement and Data Analysis, edited by Aubinet, M., Vesala, T., and Papale, D., Springer Netherlands, Dordrecht, https://doi.org/10.1007/978-94-007-2351-1, 2012.

Baldocchi, D.: Measuring Fluxes of Trace Gases and Energy between Ecosystems and the Atmosphere – the State and Future of the Eddy Covariance Method, Global Change Biology, 20, 3600–3609, https://doi.org/10.1111/gcb.12649, 2014.

Barr, A., Richardson, A., Hollinger, D., Papale, D., Arain, M., Black, T., Bohrer, G., Dragoni, D., Fischer, M., Gu, L., Law, B., Margolis, H., McCaughey, J., Munger, J., Oechel, W., and Schaeffer, K.: Use of Change-Point Detection for Friction–Velocity Threshold Evaluation in Eddy-Covariance Studies, Agricultural and Forest Meteorology, 171–172, 31–45, https://doi.org/10.1016/j.agrformet.2012.11.023, 2013.

Böhm, C., Kanzler, M., and Freese, D.: Wind Speed Reductions as Influenced by Woody Hedgerows Grown for Biomass in Short Rotation Alley Cropping Systems in Germany, Agroforestry Systems, 88, 579–591, https://doi.org/10.1007/s10457-014-9700-y, 2014.

Callejas-Rodelas, J. Á., Knohl, A., van Ramshorst, J., Mammarella, I., and Markwitz, C.: Comparison between Lower-Cost and Conventional Eddy Covariance Setups for CO_2 and Evapotranspiration Measurements above Monocropping and Agroforestry Systems, Agricultural and Forest Meteorology, 354, 110 086, https://doi.org/10.1016/j.agrformet.2024.110086, 2024.

Callejas-Rodelas, J. Á., Knohl, A., Mammarella, I., Vesala, T., Peltola, O., and Markwitz, C.: Does Increased Spatial Replication above Heterogeneous Agroforestry Improve the Representativeness of Eddy Covariance Measurements?, https://doi.org/10.5194/egusphere-2025-810, 2025a.

Callejas Rodelas, J. Á., van Ramshorst, J., Knohl, A., Siebicke, L., and Markwitz, C.: A Multiyear Eddy Covariance and Meteorological Dataset from Five Pairs of Agroforestry and Monocropping Agroecosystems in Northern Germany, https://doi.org/10.25625/A2Z8T8, 2025b.

Cardinael, R., Chevallier, T., Barthès, B. G., Saby, N. P., Parent, T., Dupraz, C., Bernoux, M., and Chenu, C.: Impact of Alley Cropping Agroforestry on Stocks, Forms and Spatial Distribution of Soil Organic Carbon — A Case Study in a Mediterranean Context, Geoderma, 259–260, 288–299, https://doi.org/10.1016/j.geoderma.2015.06.015, 2015.

Cardinael, R., Chevallier, T., Cambou, A., Béral, C., Barthès, B. G., Dupraz, C., Durand, C., Kouakoua, E., and Chenu, C.: Increased Soil Organic Carbon Stocks under Agroforestry: A Survey of Six Different Sites in France, Agriculture, Ecosystems & Environment, 236, 243–255, https://doi.org/10.1016/j.agee.2016.12.011, 2017.

Cardinael, R., Cadisch, G., Gosme, M., Oelbermann, M., and Van Noordwijk, M.: Climate Change Mitigation and Adaptation in Agriculture: Why Agroforestry Should Be Part of the Solution, Agriculture, Ecosystems & Environment, 319, 107 555, https://doi.org/10.1016/j.agee.2021.107555, 2021.

Chapman, M., Walker, W. S., Cook-Patton, S. C., Ellis, P. W., Farina, M., Griscom, B. W., and Baccini, A.: Large Climate Mitigation Potential from Adding Trees to Agricultural Lands, Global Change Biology, 26, 4357–4365, https://doi.org/10.1111/gcb.15121, 2020.

Chen, B., Coops, N. C., Fu, D., Margolis, H. A., Amiro, B. D., Barr, A. G., Black, T. A., Arain, M. A., Bourque, C. P.-A., Flanagan, L. B., Lafleur, P. M., McCaughey, J. H., and Wofsy, S. C.: Assessing Eddy-Covariance Flux Tower Location Bias across the Fluxnet-Canada Research Network Based on Remote Sensing and Footprint Modelling, Agricultural and Forest Meteorology, 151, 87–100, https://doi.org/10.1016/j.agrformet.2010.09.005, 2011.

Chen, T. and Guestrin, C.: XGBoost: A Scalable Tree Boosting System, in: Proceedings of the 22nd ACM SIGKDD International Conference on Knowledge Discovery and Data Mining, pp. 785–794, ACM, San Francisco California USA, https://doi.org/10.1145/2939672.2939785, 2016.

Chinchilla-Soto, C., Durán-Quesada, A. M., Monge-Muñoz, M., and Gutiérrez-Soto, M. V.: Quantifying the Annual Cycle of Water Use Efficiency, Energy and CO2 Fluxes Using Micrometeorological and Physiological Techniques for a Coffee Field in Costa Rica, Forests, 12, 889, https://doi.org/10.3390/f12070889, 2021.

Chu, H., Baldocchi, D. D., Poindexter, C., Abraha, M., Desai, A. R., Bohrer, G., Arain, M. A., Griffis, T., Blanken, P. D., O'Halloran, T. L., Thomas, R. Q., Zhang, Q., Burns, S. P., Frank, J. M., Christian, D., Brown, S., Black, T. A., Gough, C. M., Law, B. E., Lee, X., Chen, J., Reed, D. E., Massman, W. J., Clark, K., Hatfield, J., Prueger, J., Bracho, R., Baker, J. M., and Martin, T. A.: Temporal Dynamics of Aerodynamic Canopy Height Derived From Eddy Covariance Momentum Flux Data Across North American Flux Networks, Geophysical Research Letters, 45, 9275–9287, https://doi.org/10.1029/2018GL079306, 2018.

Crameri, F., Shephard, G. E., and Heron, P. J.: The Misuse of Colour in Science Communication, Nature Communications, 11, 5444, https://doi.org/10.1038/s41467-020-19160-7, 2020.

De Stefano, A. and Jacobson, M. G.: Soil Carbon Sequestration in Agroforestry Systems: A Meta-Analysis, Agroforestry Systems, https://doi.org/10.1007/s10457-017-0147-9, 2017.

Dee, D. P., Uppala, S. M., Simmons, A. J., Berrisford, P., Poli, P., Kobayashi, S., Andrae, U., Balmaseda, M. A., Balsamo, G., Bauer, P., Bechtold, P., Beljaars, A. C. M., Van De Berg, L., Bidlot, J., Bormann, N., Delsol, C., Dragani, R., Fuentes, M., Geer, A. J., Haimberger, L., Healy, S. B., Hersbach, H., Hólm, E. V., Isaksen, L., Kållberg, P., Köhler, M., Matricardi, M., McNally, A. P., Monge-Sanz, B. M., Morcrette, J.-J., Park, B.-K., Peubey, C., De Rosnay, P., Tavolato, C., Thépaut, J.-N., and Vitart, F.: The ERA-Interim Reanalysis: Configuration and Performance of the Data Assimilation System, Quarterly Journal of the Royal Meteorological Society, 137, 553–597, https://doi.org/10.1002/qj.828, 2011.

DWD: Deutscher Wetterdienst Climatological Means, 2024.

Dyukarev, E.: Comparison of Artificial Neural Network and Regression Models for Filling Temporal Gaps of Meteorological Variables Time Series, Applied Sciences, 13, 2646, https://doi.org/10.3390/app13042646, 2023.

El Hachimi, C., Belaqziz, S., Khabba, S., Ousanouan, Y., Sebbar, B.-e., Kharrou, M. H., and Chehbouni, A.: ClimateFiller: A Python Framework for Climate Time Series Gap-Filling and Diagnosis Based on Artificial Intelligence and Multi-Source Reanalysis Data, Software Impacts, 18, 100 575, https://doi.org/10.1016/j.simpa.2023.100575, 2023.

Finkelstein, P. L. and Sims, P. F.: Sampling Error in Eddy Correlation Flux Measurements, Journal of Geophysical Research: Atmospheres, 106, 3503–3509, https://doi.org/10.1029/2000JD900731, 2001.

Foken, T., Göockede, M., Mauder, M., Mahrt, L., Amiro, B., and Munger, W.: Post-Field Data Quality Control, in: Handbook of Micrometeorology, edited by Lee, X., Massman, W., and Law, B., vol. 29, pp. 181–208, Kluwer Academic Publishers, Dordrecht, https://doi.org/10.1007/1-4020-2265-4_9, 2005.

Göckede, M., Rebmann, C., and Foken, T.: A Combination of Quality Assessment Tools for Eddy Covariance Measurements with Footprint Modelling for the Characterisation of Complex Sites, Agricultural and Forest Meteorology, 127, 175–188, https://doi.org/10.1016/j.agrformet.2004.07.012, 2004.

Gomez-Delgado, F., Roupsard, O., Rapidel, B., Harmand, J. M., Voltz, M., Bonnefond, J. M., Imbach, P., and Moussa, R.: Modelling the Hydrological Behaviour of a Coffee Agroforestry Basin in Costa Rica, Hydrology and Earth System Sciences, 15, 369–392, https://doi.org/10.5194/hess-15-369-2011, 2011.

https://doi.org/10.5194/essd-2025-440
Preprint. Discussion started: 28 August 2025

Gupta, S. R., Dagar, J. C., and Teketay, D.: Agroforestry for Rehabilitation of Degraded Landscapes: Achieving Livelihood and Environmental Security, in: Agroforestry for Degraded Landscapes, edited by Dagar, J. C., Gupta, S. R., and Teketay, D., pp. 23–68, Springer Singapore, Singapore, https://doi.org/10.1007/978-981-15-4136-0_2, 2020.

Haiden, T., Sandu, I., Balsamo, G., Arduini, G., and Beljaars, A.: Addressing Biases in Near-Surface Forecasts, https://doi.org/10.21957/ENG71D53TH, 2018.

Hatfield, J. L. and Dold, C.: Water-Use Efficiency: Advances and Challenges in a Changing Climate, Frontiers in Plant Science, 10, 103, https://doi.org/10.3389/fpls.2019.00103, 2019.

Hersbach, H., Bell, B., Berrisford, P., Hirahara, S., Horányi, A., Muñoz-Sabater, J., Nicolas, J., Peubey, C., Radu, R., Schepers, D., Simmons, A., Soci, C., Abdalla, S., Abellan, X., Balsamo, G., Bechtold, P., Biavati, G., Bidlot, J., Bonavita, M., De Chiara, G., Dahlgren, P., Dee, D., Diamantakis, M., Dragani, R., Flemming, J., Forbes, R., Fuentes, M., Geer, A., Haimberger, L., Healy, S., Hogan, R. J., Hólm, E., Janisková, M., Keeley, S., Laloyaux, P., Lopez, P., Lupu, C., Radnoti, G., De Rosnay, P., Rozum, I., Vamborg, F., Villaume, S., and Thépaut, J.-N.: The ERA5 Global Reanalysis, Quarterly Journal of the Royal Meteorological Society, 146, 1999–2049, https://doi.org/10.1002/qj.3803, 2020.

Hersbach, H., Bell, B., Berrisford, P., Biavati, G., Horányi, A., Muñoz Sabater, J., Nicolas, J., Peubey, C., Radu, R., Rozum, I., Schepers, D., Simmons, A., Soci, C., Dee, D., and Thépaut, J.-N.: ERA5 Hourly Data on Single Levels from 1959 to Present. Copernicus Climate Change Service (C3S) Climate Data Store (CDS)., 2023.

Hill, T., Chocholek, M., and Clement, R.: The Case for Increasing the Statistical Power of Eddy Covariance Ecosystem Studies: Why, Where and How?, Global Change Biology, 23, 2154–2165, https://doi.org/10.1111/gcb.13547, 2017.

Howlett, D. S., Moreno, G., Mosquera Losada, M. R., Nair, P. K. R., and Nair, V. D.: Soil Carbon Storage as Influenced by Tree Cover in the Dehesa Cork Oak Silvopasture of Central-Western Spain, Journal of Environmental Monitoring, 13, 1897, https://doi.org/10.1039/c1em10059a, 2011.

Kanzler, M., Böhm, C., and Freese, D.: The Development of Soil Organic Carbon under Young Black Locust (Robinia Pseudoacacia L.) Trees at a Post-Mining Landscape in Eastern Germany, New Forests, 52, 47–68, https://doi.org/10.1007/s11056-020-09779-1, 2021.

Kay, S., Rega, C., Moreno, G., Den Herder, M., Palma, J. H., Borek, R., Crous-Duran, J., Freese, D., Giannitsopoulos, M., Graves, A., Jäger, M., Lamersdorf, N., Memedemin, D., Mosquera-Losada, R., Pantera, A., Paracchini, M. L., Paris, P., Roces-Díaz, J. V., Rolo, V., Rosati, A., Sandor, M., Smith, J., Szerencsits, E., Varga, A., Viaud, V., Wawer, R., Burgess, P. J., and Herzog, F.: Agroforestry Creates Carbon Sinks Whilst Enhancing the Environment in Agricultural Landscapes in Europe, Land Use Policy, 83, 581–593, https://doi.org/10.1016/j.landusepol.2019.02.025, 2019.

Kessomkiat, W., Franssen, H.-J. H., Graf, A., and Vereecken, H.: Estimating Random Errors of Eddy Covariance Data: An Extended Two-Tower Approach, Agricultural and Forest Meteorology, 171–172, 203–219, https://doi.org/10.1016/j.agrformet.2012.11.019, 2013.

Kljun, N., Calanca, P., Rotach, M. W., and Schmid, H. P.: A Simple Two-Dimensional Parameterisation for Flux Footprint Prediction (FFP), Geoscientific Model Development, 8, 3695–3713, https://doi.org/10.5194/gmd-8-3695-2015, 2015.

Langhof, M. and Swieter, A.: Five Years of Grassland Yield and Quality Assessment in a Temperate Short-Rotation Alley Cropping Agroforestry System, Agroforestry Systems, 98, 933–937, https://doi.org/10.1007/s10457-024-00963-2, 2024.

Lasslop, G., Reichstein, M., Papale, D., Richardson, A. D., Arneth, A., Barr, A., Stoy, P., and Wohlfahrt, G.: Separation of Net Ecosystem Exchange into Assimilation and Respiration Using a Light Response Curve Approach: Critical Issues and Global Evaluation, Global Change Biology, 16, 187–208, https://doi.org/10.1111/j.1365-2486.2009.02041.x, 2010.

Leys, C., Ley, C., Klein, O., Bernard, P., and Licata, L.: Detecting Outliers: Do Not Use Standard Deviation around the Mean, Use Absolute Deviation around the Median, Journal of Experimental Social Psychology, 49, 764–766, https://doi.org/10.1016/j.jesp.2013.03.013, 2013.

Lipson, M., Grimmond, S., Best, M., Chow, W. T. L., Christen, A., Chrysoulakis, N., Coutts, A., Crawford, B., Earl, S., Evans, J., Fortuniak, K., Heusinkveld, B. G., Hong, J.-W., Hong, J., Järvi, L., Jo, S., Kim, Y.-H., Kotthaus, S., Lee, K., Masson, V., McFadden, J. P., Michels, O., Pawlak, W., Roth, M., Sugawara, H., Tapper, N., Velasco, E., and Ward, H. C.: Harmonized Gap-Filled Datasets from 20 Urban Flux Tower Sites, Earth System Science Data, 14, 5157–5178, https://doi.org/10.5194/essd-14-5157-2022, 2022.

Liu, Y., Lucas, B., Bergl, D. D., and Richardson, A. D.: Robust Filling of Extra-Long Gaps in Eddy Covariance CO2 Flux Measurements from a Temperate Deciduous Forest Using eXtreme Gradient Boosting, Agricultural and Forest Meteorology, 364, 110 438, https://doi.org/10.1016/j.agrformet.2025.110438, 2025.

Lucarini, A., Cascio, M. L., Marras, S., Sirca, C., and Spano, D.: Artificial Intelligence and Eddy Covariance: A Review, Science of The Total Environment, 950, 175 406, https://doi.org/10.1016/j.scitotenv.2024.175406, 2024.

Lucas-Moffat, A. M., Schrader, F., Herbst, M., and Brümmer, C.: Multiple Gap-Filling for Eddy Covariance Datasets, Agricultural and Forest Meteorology, 325, 109 114, https://doi.org/10.1016/j.agrformet.2022.109114, 2022.

Mahabbati, A., Beringer, J., Leopold, M., McHugh, I., Cleverly, J., Isaac, P., and Izady, A.: A Comparison of Gap-Filling Algorithms for Eddy Covariance Fluxes and Their Drivers, Geoscientific Instrumentation, Methods and Data Systems, 10, 123–140, https://doi.org/10.5194/gi-10-123-2021, 2021.

Mammarella, I., Launiainen, S., Gronholm, T., Keronen, P., Pumpanen, J., Rannik, Ü., and Vesala, T.: Relative Humidity Effect on the High-Frequency Attenuation of Water Vapor Flux Measured by a Closed-Path Eddy Covariance System, Journal of Atmospheric and Oceanic Technology, 26, 1856–1866, https://doi.org/10.1175/2009JTECHA1179.1, 2009.

Mammarella, I., Peltola, O., Nordbo, A., Järvi, L., and Rannik, Ü.: Quantifying the Uncertainty of Eddy Covariance Fluxes Due to the Use of Different Software Packages and Combinations of Processing Steps in Two Contrasting Ecosystems, Atmospheric Measurement Techniques, 9, 4915–4933, https://doi.org/10.5194/amt-9-4915-2016, 2016.

Markwitz, C. and Siebicke, L.: Low-Cost Eddy Covariance: A Case Study of Evapotranspiration over Agroforestry in Germany, Atmospheric Measurement Techniques, 12, 4677–4696, https://doi.org/10.5194/amt-12-4677-2019, 2019.

Markwitz, C., Knohl, A., and Siebicke, L.: Evapotranspiration over Agroforestry Sites in Germany, Biogeosciences, 17, 5183–5208, https://doi.org/10.5194/bg-17-5183-2020, 2020a.

Markwitz, C., Knohl, A., and Siebicke, L.: Data Set Supporting Journal Article: Markwitz, C., Knohl, A. and Siebicke, L.: "Evapotranspiration over Agroforestry Sites in Germany", Biogeosciences, https://doi.org/10.5281/ZENODO.4038398, 2020b.

Massman, W. and Lee, X.: Eddy Covariance Flux Corrections and Uncertainties in Long-Term Studies of Carbon and Energy Exchanges, Agricultural and Forest Meteorology, 113, 121–144, https://doi.org/10.1016/S0168-1923(02)00105-3, 2002.

Mauder, M., Cuntz, M., Drüe, C., Graf, A., Rebmann, C., Schmid, H. P., Schmidt, M., and Steinbrecher, R.: A Strategy for Quality and Uncertainty Assessment of Long-Term Eddy-Covariance Measurements, Agricultural and Forest Meteorology, 169, 122–135, https://doi.org/10.1016/j.agrformet.2012.09.006, 2013.

Moffat, A. M., Papale, D., Reichstein, M., Hollinger, D. Y., Richardson, A. D., Barr, A. G., Beckstein, C., Braswell, B. H., Churkina, G., Desai, A. R., Falge, E., Gove, J. H., Heimann, M., Hui, D., Jarvis, A. J., Kattge, J., Noormets, A., and Stauch, V. J.: Comprehensive Comparison of Gap-Filling Techniques for Eddy Covariance Net Carbon Fluxes, Agricultural and Forest Meteorology, 147, 209–232, https://doi.org/10.1016/j.agrformet.2007.08.011, 2007.

https://doi.org/10.5194/essd-2025-440
Preprint. Discussion started: 28 August 2025

Muñoz-Sabater, J., Dutra, E., Agustí-Panareda, A., Albergel, C., Arduini, G., Balsamo, G., Boussetta, S., Choulga, M., Harrigan, S., Hersbach, H., Martens, B., Miralles, D. G., Piles, M., Rodríguez-Fernández, N. J., Zsoter, E., Buontempo, C., and Thépaut, J.-N.: ERA5-Land: A State-of-the-Art Global Reanalysis Dataset for Land Applications, Earth System Science Data, 13, 4349–4383, https://doi.org/10.5194/essd-13-4349-2021, 2021.

Murray, F. W.: On the Computation of Saturation Vapor Pressure, Journal of Applied Meteorology, 6, 203–204, https://doi.org/10.1175/1520-0450(1967)006<0203:OTCOSV>2.0.CO;2, 1967.

Nair, P. K. R.: Classification of Agroforestry Systems, Agroforestry Systems, 3, 97–128, https://doi.org/10.1007/bf00122638, 1985.

Ong, C., Wilson, J., Deans, J., Mulayta, J., Raussen, T., and Wajja-Musukwe, N.: Tree–Crop Interactions: Manipulation of Water Use and Root Function, Agricultural Water Management, 53, 171–186, https://doi.org/10.1016/S0378-3774(01)00163-9, 2002.

Pancholi, R., Yadav, R., Gupta, H., Vasure, N., Choudhary, S., Singh, M. N., and Rastogi, M.: The Role of Agroforestry Systems in Enhancing Climate Resilience and Sustainability- A Review, International Journal of Environment and Climate Change, 13, 4342–4353, https://doi.org/10.9734/IJECC/2023/v13i113615, 2023.

Papale, D., Reichstein, M., Aubinet, M., Canfora, E., Bernhofer, C., Kutsch, W., Longdoz, B., Rambal, S., Valentini, R., Vesala, T., and Yakir, D.: Towards a Standardized Processing of Net Ecosystem Exchange Measured with Eddy Covariance Technique: Algorithms and Uncertainty Estimation, Biogeosciences (Online), 3, 571–583, https://doi.org/10.5194/bg-3-571-2006, 2006.

Pastorello, G., Trotta, C., Canfora, E., Chu, H., Christianson, D., Cheah, Y.-W., Poindexter, C., Chen, J., Elbashandy, A., Humphrey, M., Isaac, P., Polidori, D., Reichstein, M., Ribeca, A., Van Ingen, C., Vuichard, N., Zhang, L., Amiro, B., Ammann, C., Arain, M. A., Ardö, J., Arkebauer, T., Arndt, S. K., Arriga, N., Aubinet, M., Aurela, M., Baldocchi, D., Barr, A., Beamesderfer, E., Marchesini, L. B., Bergeron, O., Beringer, J., Bernhofer, C., Berveiller, D., Billesbach, D., Black, T. A., Blanken, P. D., Bohrer, G., Boike, J., Bolstad, P. V., Bonal, D., Bonnefond, J.-M., Bowling, D. R., Bracho, R., Brodeur, J., Brümmer, C., Buchmann, N., Burban, B., Burns, S. P., Buysse, P., Cale, P., Cavagna, M., Cellier, P., Chen, S., Chini, I., Christensen, T. R., Cleverly, J., Collalti, A., Consalvo, C., Cook, B. D., Cook, D., Coursolle, C., Cremonese, E., Curtis, P. S., D'Andrea, E., Da Rocha, H., Dai, X., Davis, K. J., Cinti, B. D., Grandcourt, A. D., Ligne, A. D., De Oliveira, R. C., Delpierre, N., Desai, A. R., Di Bella, C. M., Tommasi, P. D., Dolman, H., Domingo, F., Dong, G., Dore, S., Duce, P., Dufrêne, E., Dunn, A., Dušek, J., Eamus, D., Eichelmann, U., ElKhidir, H. A. M., Eugster, W., Ewenz, C. M., Ewers, B., Famulari, D., Fares, S., Feigenwinter, I., Feitz, A., Fensholt, R., Filippa, G., Fischer, M., Frank, J., Galvagno, M., Gharun, M., Gianelle, D., Gielen, B., Gioli, B., Gitelson, A., Goded, I., Goeckede, M., Goldstein, A. H., Gough, C. M., Goulden, M. L., Graf, A., Griebel, A., Gruening, C., Grünwald, T., Hammerle, A., Han, S., Han, X., Hansen, B. U., Hanson, C., Hatakka, J., He, Y., Hehn, M., Heinesch, B., Hinko-Najera, N., Hörtnagl, L., Hutley, L., Ibrom, A., Ikawa, H., Jackowicz-Korczynski, M., Janouš, D., Jans, W., Jassal, R., Jiang, S., Kato, T., Khomik, M., Klatt, J., Knohl, A., Knox, S., Kobayashi, H., Koerber, G., Kolle, O., Kosugi, Y., Kotani, A., Kowalski, A., Kruijt, B., Kurbatova, J., Kutsch, W. L., Kwon, H., Launiainen, S., Laurila, T., Law, B., Leuning, R., Li, Y., Liddell, M., Limousin, J.-M., Lion, M., Liska, A. J., Lohila, A., López-Ballesteros, A., López-Blanco, E., Loubet, B., Loustau, D., Lucas-Moffat, A., Lüers, J., Ma, S., Macfarlane, C., Magliulo, V., Maier, R., Mammarella, I., Manca, G., Marcolla, B., Margolis, H. A., Marras, S., Massman, W., Mastepanov, M., Matamala, R., Matthes, J. H., Mazzenga, F., McCaughey, H., McHugh, I., McMillan, A. M. S., Merbold, L., Meyer, W., Meyers, T., Miller, S. D., Minerbi, S., Moderow, U., Monson, R. K., Montagnani, L., Moore, C. E., Moors, E., Moreaux, V., Moureaux, C., Munger, J. W., Nakai, T., Neirynck, J., Nesic, Z., Nicolini, G., Noormets, A., Northwood, M., Nosetto, M., Nouvellon, Y., Novick, K., Oechel, W., Olesen, J. E., Ourcival, J.-M., Papuga, S. A., Parmentier, F.-J., Paul-Limoges, E., Pavelka, M., Peichl, M., Pendall, E., Phillips, R. P., Pilegaard, K., Pirk, N., Posse, G., Powell, T., Prasse, H., Prober, S. M., Rambal, S., Rannik, Ü., Raz-Yaseef, N., Rebmann, C., Reed, D., Dios, V. R. D., Restrepo-Coupe, N., Reverter, B. R., Roland, M., Sabbatini, S., Sachs, T., Saleska, S. R., Sánchez-Cañete, E. P., Sanchez-Mejia, Z. M., Schmid, H. P.,

https://doi.org/10.5194/essd-2025-440
Preprint. Discussion started: 28 August 2025

Schmidt, M., Schneider, K., Schrader, F., Schroder, I., Scott, R. L., Sedlák, P., Serrano-Ortíz, P., Shao, C., Shi, P., Shironya, I., Siebicke, L., Šigut, L., Silberstein, R., Sirca, C., Spano, D., Steinbrecher, R., Stevens, R. M., Sturtevant, C., Suyker, A., Tagesson, T., Takanashi, S., Tang, Y., Tapper, N., Thom, J., Tomassucci, M., Tuovinen, J.-P., Urbanski, S., Valentini, R., Van Der Molen, M., Van Gorsel, E., Van Huissteden, K., Varlagin, A., Verfaillie, J., Vesala, T., Vincke, C., Vitale, D., Vygodskaya, N., Walker, J. P., Walter-Shea, E., Wang, H., Weber, R., Westermann, S., Wille, C., Wofsy, S., Wohlfahrt, G., Wolf, S., Woodgate, W., Li, Y., Zampedri, R., Zhang, J., Zhou, G., Zona, D., Agarwal, D., Biraud, S., Torn, M., and Papale, D.: The FLUXNET2015 Dataset and the ONEFlux Processing Pipeline for Eddy Covariance Data, Scientific Data, 7, 225, https://doi.org/10.1038/s41597-020-0534-3, 2020.

Pedregosa, F., Varoquaux, G., Gramfort, A., Michel, V., Thirion, B., Grisel, O., Blondel, M., Müller, A., Nothman, J., Louppe, G., Prettenhofer, P., Weiss, R., Dubourg, V., Vanderplas, J., Passos, A., Cournapeau, D., Brucher, M., Perrot, M., and Duchesnay, \.: Scikit-Learn: Machine Learning in Python, https://doi.org/10.48550/ARXIV.1201.0490, 2012.

Peichl, M., Thevathasan, N. V., Gordon, A. M., Huss, J., and Abohassan, R. A.: Carbon Sequestration Potentials in Temperate Tree-Based Intercropping Systems, Southern Ontario, Canada, Agroforestry Systems, 66, 243–257, https://doi.org/10.1007/s10457-005-0361-8, 2006.

Quinkenstein, A., Wöllecke, J., Böhm, C., Grünewald, H., Freese, D., Schneider, B. U., and Hüttl, R. F.: Ecological Benefits of the Alley Cropping Agroforestry System in Sensitive Regions of Europe, Environmental Science & Policy, 12, 1112–1121, https://doi.org/10.1016/j.envsci.2009.08.008, 2009.

Rannik, Ü. and Vesala, T.: Autoregressive Filtering versus Linear Detrending in Estimation of Fluxes by the Eddy Covariance Method, Boundary-Layer Meteorology, 91, 259–280, https://doi.org/10.1023/A:1001840416858, 1999.

Rebmann, C., Göckede, M., Foken, T., Aubinet, M., Aurela, M., Berbigier, P., Bernhofer, C., Buchmann, N., Carrara, A., Cescatti, A., Ceulemans, R., Clement, R., Elbers, J. A., Granier, A., Grünwald, T., Guyon, D., Havránková, K., Heinesch, B., Knohl, A., Laurila, T., Longdoz, B., Marcolla, B., Markkanen, T., Miglietta, F., Moncrieff, J., Montagnani, L., Moors, E., Nardino, M., Ourcival, J.-M., Rambal, S., Rannik, Ü., Rotenberg, E., Sedlak, P., Unterhuber, G., Vesala, T., and Yakir, D.: Quality Analysis Applied on Eddy Covariance Measurements at Complex Forest Sites Using Footprint Modelling, Theoretical and Applied Climatology, 80, 121–141, https://doi.org/10.1007/s00704-004-0095-y, 2005.

Rebmann, C., Aubinet, M., Schmid, H., Arriga, N., Aurela, M., Burba, G., Clement, R., De Ligne, A., Fratini, G., Gielen, B., Grace, J., Graf, A., Gross, P., Haapanala, S., Herbst, M., Hörtnagl, L., Ibrom, A., Joly, L., Kljun, N., Kolle, O., Kowalski, A., Lindroth, A., Loustau, D., Mammarella, I., Mauder, M., Merbold, L., Metzger, S., Mölder, M., Montagnani, L., Papale, D., Pavelka, M., Peichl, M., Roland, M., Serrano-Ortiz, P., Siebicke, L., Steinbrecher, R., Tuovinen, J.-P., Vesala, T., Wohlfahrt, G., and Franz, D.: ICOS Eddy Covariance Flux-Station Site Setup: A Review, International Agrophysics, 32, 471–494, https://doi.org/10.1515/intag-2017-0044, 2018.

Reichstein, M., Falge, E., Baldocchi, D., Papale, D., Aubinet, M., Berbigier, P., Bernhofer, C., Buchmann, N., Gilmanov, T., Granier, A., Grünwald, T., Havránková, K., Ilvesniemi, H., Janous, D., Knohl, A., Laurila, T., Lohila, A., Loustau, D., Matteucci, G., Meyers, T., Miglietta, F., Ourcival, J.-M., Pumpanen, J., Rambal, S., Rotenberg, E., Sanz, M., Tenhunen, J., Seufert, G., Vaccari, F., Vesala, T., Yakir, D., and Valentini, R.: On the Separation of Net Ecosystem Exchange into Assimilation and Ecosystem Respiration: Review and Improved Algorithm, Global Change Biology, 11, 1424–1439, https://doi.org/10.1111/j.1365-2486.2005.001002.x, 2005.

Richardson, A. D. and Hollinger, D. Y.: A Method to Estimate the Additional Uncertainty in Gap-Filled NEE Resulting from Long Gaps in the CO2 Flux Record, Agricultural and Forest Meteorology, 147, 199–208, https://doi.org/10.1016/j.agrformet.2007.06.004, 2007.

Richardson, A. D., Mahecha, M. D., Falge, E., Kattge, J., Moffat, A. M., Papale, D., Reichstein, M., Stauch, V. J., Braswell, B. H., Churkina, G., Kruijt, B., and Hollinger, D. Y.: Statistical Properties of Random CO2 Flux Measurement Uncertainty Inferred from Model Residuals, Agricultural and Forest Meteorology, 148, 38–50, https://doi.org/10.1016/j.agrformet.2007.09.001, 2008.

Sabbatini, S., Mammarella, I., Arriga, N., Fratini, G., Graf, A., Hörtnagl, L., Ibrom, A., Longdoz, B., Mauder, M., Merbold, L., Metzger, S., Montagnani, L., Pitacco, A., Rebmann, C., Sedlák, P., Šigut, L., Vitale, D., and Papale, D.: Eddy Covariance Raw Data Processing for CO2 and Energy Fluxes Calculation at ICOS Ecosystem Stations, International Agrophysics, 32, 495–515, https://doi.org/10.1515/intag-2017-0043, 2018.

Satish, P., Madiwalar, A. F., Lallawmkimi, M. C., Reddy, K. J., Parveen, S., P, A., Laxman, T., Kiruba, M., and Anand, G.: Agroforestry: Multifunctional Benefits and Implementation Strategies, Journal of Geography, Environment and Earth Science International, 28, 1–12, https://doi.org/10.9734/jgeesi/2024/v28i10821, 2024.

Schimel, D., Pavlick, R., Fisher, J. B., Asner, G. P., Saatchi, S., Townsend, P., Miller, C., Frankenberg, C., Hibbard, K., and Cox, P.: Observing Terrestrial Ecosystems and the Carbon Cycle from Space, Global Change Biology, 21, 1762–1776, https://doi.org/10.1111/gcb.12822, 2015.

Schmidt, M., Corre, M. D., Kim, B., Morley, J., Göbel, L., Sharma, A. S. I., Setriuc, S., and Veldkamp, E.: Nutrient Saturation of Crop Monocultures and Agroforestry Indicated by Nutrient Response Efficiency, Nutrient Cycling in Agroecosystems, 119, 69–82, https://doi.org/10.1007/s10705-020-10113-6, 2021.

Shao, G., Martinson, G. O., Corre, M. D., Luo, J., Niu, D., and Veldkamp, E.: Conversion of Cropland Monoculture to Agroforestry Increases Methane Uptake, Agronomy for Sustainable Development, 45, 1, https://doi.org/10.1007/s13593-024-00997-x, 2025.

Singh, V., Johar, V., Kumar, R., and Chaudhary, M.: Socio-Economic and Environmental Assets Sustainability by Agroforestry Systems: A Review, International Journal of Agriculture, Environment and Biotechnology, 14, 521–533, https://doi.org/10.30954/0974-1712.04.2021.6, 2021.

Sprenkle-Hyppolite, S., Griscom, B., Griffey, V., Munshi, E., and Chapman, M.: Maximizing Tree Carbon in Croplands and Grazing Lands While Sustaining Yields, Carbon Balance and Management, 19, 23, https://doi.org/10.1186/s13021-024-00268-y, 2024.

Tikkasalo, O.-P., Peltola, O., Alekseychik, P., Heikkinen, J., Launiainen, S., Lehtonen, A., Li, Q., Martínez-García, E., Peltoniemi, M., Salovaara, P., Tuominen, V., and Mäkipää, R.: Eddy-Covariance Fluxes of CO_2 , CH_4 and N_2 O in a Drained Peatland Forest after Clear-Cutting, Biogeosciences, 22, 1277–1300, https://doi.org/10.5194/bg-22-1277-2025, 2025.

Tramontana, G., Jung, M., Schwalm, C. R., Ichii, K., Camps-Valls, G., Ráduly, B., Reichstein, M., Arain, M. A., Cescatti, A., Kiely, G., Merbold, L., Serrano-Ortiz, P., Sickert, S., Wolf, S., and Papale, D.: Predicting Carbon Dioxide and Energy Fluxes across Global FLUXNET Sites Withregression Algorithms, Biogeosciences (Online), 13, 4291–4313, https://doi.org/10.5194/bg-13-4291-2016, 2016.

van Gorsel, E., Delpierre, N., Leuning, R., Black, A., Munger, J. W., Wofsy, S., Aubinet, M., Feigenwinter, C., Beringer, J., Bonal, D., Chen, B., Chen, J., Clement, R., Davis, K. J., Desai, A. R., Dragoni, D., Etzold, S., Grünwald, T., Gu, L., Heinesch, B., Hutyra, L. R., Jans, W. W., Kutsch, W., Law, B., Leclerc, M. Y., Mammarella, I., Montagnani, L., Noormets, A., Rebmann, C., and Wharton, S.: Estimating Nocturnal Ecosystem Respiration from the Vertical Turbulent Flux and Change in Storage of CO2, Agricultural and Forest Meteorology, 149, 1919–1930, https://doi.org/10.1016/j.agrformet.2009.06.020, 2009.

van Ramshorst, J. G. V., Knohl, A., Callejas-Rodelas, J. Á., Clement, R., Hill, T. C., Siebicke, L., and Markwitz, C.: Lower-Cost Eddy Covariance for CO_2 and H_2 O Fluxes over Grassland and Agroforestry, Atmospheric Measurement Techniques, 17, 6047–6071, https://doi.org/10.5194/amt-17-6047-2024, 2024.

van Ramshorst, J. G. V., Callejas-Rodelas, J. Á., Knohl, A., and Markwitz, C.: Comparison of Ecosystem-Scale Carbon Fluxes at Agroforestry and Adjacent Monocropping Sites in Germany, Agroforestry Systems, 99, 147, https://doi.org/10.1007/s10457-025-01244-2, 2025.

https://doi.org/10.5194/essd-2025-440
Preprint. Discussion started: 28 August 2025

Vekuri, H., Tuovinen, J.-P., Kulmala, L., Papale, D., Kolari, P., Aurela, M., Laurila, T., Liski, J., and Lohila, A.: A Widely-Used Eddy Covariance Gap-Filling Method Creates Systematic Bias in Carbon Balance Estimates, Scientific Reports, 13, 1720, https://doi.org/10.1038/s41598-023-28827-2, 2023.

Veldkamp, E., Schmidt, M., Markwitz, C., Beule, L., Beuschel, R., Biertümpfel, A., Bischel, X., Duan, X., Gerjets, R., Göbel, L., Graß, R., Guerra, V., Heinlein, F., Komainda, M., Langhof, M., Luo, J., Potthoff, M., Van Ramshorst, J. G. V., Rudolf, C., Seserman, D.-M., Shao, G., Siebicke, L., Svoboda, N., Swieter, A., Carminati, A., Freese, D., Graf, T., Greef, J. M., Isselstein, J., Jansen, M., Karlovsky, P., Knohl, A., Lamersdorf, N., Priesack, E., Wachendorf, C., Wachendorf, M., and Corre, M. D.: Multifunctionality of Temperate Alley-Cropping Agroforestry Outperforms Open Cropland and Grassland, Communications Earth & Environment, 4, 20, https://doi.org/10.1038/s43247-023-00680-1, 2023.

Vuichard, N. and Papale, D.: Filling the Gaps in Meteorological Continuous Data Measured at FLUXNET Sites with ERA-Interim Reanalysis, Earth System Science Data, 7, 157–171, https://doi.org/10.5194/essd-7-157-2015, 2015.

Ward, P., Micin, S., and Fillery, I.: Application of Eddy Covariance to Determine Ecosystem-Scale Carbon Balance and Evapotranspiration in an Agroforestry System, Agricultural and Forest Meteorology, 152, 178–188, https://doi.org/10.1016/j.agrformet.2011.09.016, 2012.

Wilczak, J. M., Oncley, S. P., and Stage, S. A.: Sonic Anemometer Tilt Correction Algorithms, Boundary-Layer Meteorology, 99, 127–150, https://doi.org/10.1023/A:1018966204465, 2001.

Winck, B. R., Bloor, J. M. G., and Klumpp, K.: Eighteen Years of Upland Grassland Carbon Flux Data: Reference Datasets, Processing, and Gap-Filling Procedure, Scientific Data, 10, 311, https://doi.org/10.1038/s41597-023-02221-z, 2023.

Wutzler, T., Lucas-Moffat, A., Migliavacca, M., Knauer, J., Sickel, K., Šigut, L., Menzer, O., and Reichstein, M.: Basic and Extensible Post-Processing of Eddy Covariance Flux Data with REddyProc, Biogeosciences (Online), 15, 5015–5030, https://doi.org/10.5194/bg-15-5015-2018, 2018.

Zhu, S., Clement, R., McCalmont, J., Davies, C. A., and Hill, T.: Stable Gap-Filling for Longer Eddy Covariance Data Gaps: A Globally Validated Machine-Learning Approach for Carbon Dioxide, Water, and Energy Fluxes, Agricultural and Forest Meteorology, 314, 108 777, https://doi.org/10.1016/j.agrformet.2021.108777, 2022.

Zomer, R. J., Neufeldt, H., Xu, J., Ahrends, A., Bossio, D., Trabucco, A., Van Noordwijk, M., and Wang, M.: Global Tree Cover and Biomass Carbon on Agricultural Land: The Contribution of Agroforestry to Global and National Carbon Budgets, Scientific Reports, 6, 29 987, https://doi.org/10.1038/srep29987, 2016.